Tropospheric Ozone Seasonal and Long-term Variability as seen by lidar and surface measurements at the JPL-Table Mountain Facility, California

M. J. Granados-Muñoz and T. Leblanc

Jet Propulsion Laboratory, California Institute of Technology

Abstract

A combined surface and tropospheric ozone climatology and interannual variability study was performed for the first time using co-located ozone photometer measurements (2013-2015) and tropospheric ozone differential absorption lidar measurements (2000-2015) at the Jet Propulsion Laboratory Table Mountain Facility (TMF, elev. 2285 m), in California.

The surface time-series were investigated both in terms of seasonal and diurnal variability. The observed surface ozone is typical of high-elevation remote-sites, with small amplitude of the seasonal and diurnal cycles, and high ozone values, compared to neighboring lower altitude stations representative of urban boundary layer conditions. The ozone mixing ratio ranges from 45 ppbv in the winter morning hours to 65 ppbv in the spring and summer afternoon hours. At the time of the lidar measurements (early night), the seasonal cycle observed at the surface is similar to that observed by lidar between 3.5 km and 9 km.

Above 9 km, the local tropopause height variation with time and season impacts significantly the ozone lidar observations. The frequent tropopause folds found in the vicinity of TMF (27% of the time in winter and spring) produce a dual-peak vertical structure in ozone within the fold layer,
characterized by higher-than-average values in the bottom half of the fold (12-14 km), and lower-than-averaged values in the top half of the fold (14-18 km). This structure is consistent with the expected origin of the air parcels within the fold, i.e., mid-latitude stratospheric air folding down below the upper tropospheric sub-tropical air.

No significant signature of interannual variability could be observed on the 2000-2015 deseasonalized lidar time-series, with only a statistically non-significant positive anomaly during the years 2003-2007. Our trend analysis reveals however a statistically significant positive trend of 0.3~~1~~ ppbv.year^{-1} ~~i~~(0.6%) in the free troposphere (7-10 km) for the period 2000-2015.

A classification of the air parcels sampled by lidar was made at 1-km intervals between 5 km and 14 km altitude, using 8-days backward trajectories (HYSPLIT). Our classification revealed the large influence of the Pacific Ocean, with air parcels of low ozone content (50-65 ppbv), and significant influence of the stratosphere leading to ozone values of 65-80 ppbv down to 8-9 km. In summer, enhanced ozone values (70 ppbv) were found in air parcels originating from Central

America, probably ~~owed~~ due to the enhanced thunderstorm activity during the North American

Monsoon. No outstanding influence from Asia was identified. <see comments in review>

1. Introduction

Ozone is an important constituent in the troposphere, impacting climate, chemistry, and air quality (The Royal Society, 2008). As a greenhouse gas (Forster et al., 2007), it contributes to the Earth's global warming with an estimate radiative forcing of 0.40 ± 0.20 W·m^{-2} (IPCC 2013). It is one of the main oxidants in the troposphere (Monks, 2005), and, in high concentrations, it can cause problems in human health and vegetation (World Health Organization, 2003). Tropospheric ozone can be directly emitted to the troposphere <how? Is there really a direct tropospheric emission source besides the stratosphere mentioned below?>, but it is primarily formed as a secondary pollutant in chemicals reactions involving ozone precursors such as methane, CO, NOx, VOCs or PANs. An additional source of ozone in the troposphere is the downward transport from the stratosphere, where ozone is much more abundant (Levy et al., 1985). At high elevation sites such as the Jet Propulsion Laboratory Table Mountain Facility in Southern California (TMF hereafter), the effect of the boundary layer is very small~~,~~ and ozone variability is expected to be driven by transport processes from the stratosphere or horizontal transport within the troposphere (Cui et al., 2009; Naja et al., 2003; Trickl et al., 2010).

Several studies show that background ozone levels have increased significantly since preindustrial times (Mickley et al., 2001; Parrish et al., 2012; Staehelin et al., 1994; Volz and Kley, 1988) and these levels continued rising in the last decades in both Hemispheres (Derwent et al., 2007; Jaffe et al., 2004; Lee and Akimoto, 1998; Naja and Akimoto, 2004; Oltmans et al., 2006; Parrish et al., 2012; Simmonds et al., 2004; Tanimoto et al., 2009; Zbinden et al., 2006; Lelieveld et al., 2004). Nevertheless, after air quality regulations were implemented in the 1970s, the increasing trend has slowed down or is even ~~reverted~~ reversed in regions such as the Eastern U.S. and Europe (Cooper et al., 2012, 2014; Granier et al., 2011). The situation is not the same for emerging economies such as Asia, where emissions are increasing with ~~the~~ a corresponding increase in ozone levels (Dufour et al., 2010; Gao et al., 2005; Strode et al., 2015; Tie et al., 2009; Wang et al., 2006).

In most cases, variability and trend studies have revealed very large ozone variability with time, location and altitude (Cooper et al., 2014). This variability is mostly due to the large heterogeneity and variability of the ozone sources themselves, the different chemical processes affecting the formation and depletion of tropospheric ozone and its variable lifetime in the troposphere. Ozone atmospheric lifetime goes from a few hours in polluted boundary layer to

several weeks in the free troposphere, allowing it to travel over distances of intercontinental scale (Stevenson et al., 2006; Young et al., 2013). In order to obtain statistically significant results and be able to assess tropospheric ozone interannual variability and trends, a large long-term monitoring dataset with global coverage is required. ~~, which~~Such a dataset has not yet been achieved with ~~considering the~~ current observation capabilities.

Long-term records of tropospheric ozone are available since the 1950s (Feister and Warmbt, 1987; Parrish et al., 2012), but it is not until the 1970s that the number of ozone monitoring stations became significant (Cooper et al., 2014 and references therein). Currently, a considerable number of ozone monitoring sites are operating as part of regional networks or international programs (e.g., World Meteorological Observation Global Atmosphere Watch WMO/GAW, Acid Deposition Monitoring Network in East Asia EANET, Clean Air Status and Trends Network CASTNET, etc.). In addition to these ground-based networks, tropospheric ozone measurements from satellite (TOMS, TES, OMI, etc.) or aircraft (MOZAIC/IAGOS) platforms have been successfully implemented. Nevertheless, most of the tropospheric ozone measurements are still only surface or column-integrated measurements whilst the number of them with information on the vertical coordinate is very ~~scarce~~small. Until ~~today~~recently, mainly ozonesonde profiles have been used to provide altitude-resolved ozone variability information in the troposphere (Logan, 1994; Logan et al., 1999; Naja and Akimoto, 2004; Oltmans et al., 1998, 2006, 2013,[*Newchurch et al.*, 2003]), but the ~~somewhat elevated~~ cost of an ozonesonde launch has kept the sampling interval to one profile per week (or less) for ~~a given~~most locations. Differential Absorption Lidar (DIAL) systems, which started to be used to measure tropospheric ozone in the late 1970s (Bufton et al., 1979 [*Proffitt and Langford*, 1997]), complement the ozonesonde records, providing higher temporal resolution thanks to their inherent operational configuration (from minutes to days of continuous measurements). ~~Today~~Currently, tropospheric ozone lidars are still very scarce, but the implementation of observation networks such as the international Network for the Detection of Atmospheric Composition Change (NDACC, http://www.ndsc.ncep.noaa.gov), and more recently the North American-based Tropospheric Ozone Lidar Network (TOLNet, http://www-air.larc.nasa.gov/missions/TOLNet) allows for new capabilities that can contribute to the understanding of processes affecting tropospheric ozone variability, and to satellite and model validation and improvement.

Formatted: Font color: Blue

Formatted: Font color: Blue

Formatted: Font color: Blue

As part of NDACC and TOLNet, a tropospheric ozone DIAL system located at TMF has been operating since 1999. In this study, an analysis of 16 years of lidar profiles measured at the station is presented together with the analysis of the surface ozone measurements available at the site since 2013. The objective is to provide the first-ever published study of tropospheric ozone variability above TMF using both the surface and lidar datasets. The work presented here is particularly valuable due to the rising interest in the detection of long-term trends in the Western United States (U.S.) and the scarcity of long-term measurements of ozone vertical profiles in this region. The high~~-~~terrain elevation and the deep planetary boundary layer of the intermountain Western U.S. region facilitate inflow of polluted air masses originating in the Asian boundary layer and ozone-rich stratospheric air down to the surface~~;~~, thus, highly influencing air quality in the region (Brown-Steiner and Hess, 2011; Cooper et al., 2004; Langford et al., 2012; Liang et al., 2004; Lin et al., 2012a, 2012b; Stohl, 2002). After a brief description of the instrumentation and datasets (Section 2), an analysis of the seasonal and interannual variability of tropospheric ozone above TMF for the period 2000-2015 will be presented in section 3. The study includes a characterization of the air parcels sampled by lidar by identification of the source regions based on backward trajectories analysis. A summary and discussion are provided in Section 4.

2. Instrumentation

2.1 Tropospheric ozone lidar

TMF is located in the San Gabriel Mountains, in Southern California (34.4◦ N, 117.7◦ W), at an elevation of 2285 m above sea level. Two differential absorption lidars (DIAL) and one Raman lidar have been operating at the facility during nighttime typically four times per week, two hours per night, contributing stratospheric ozone, temperature, tropospheric ozone, and water vapor measurements to NDACC for several decades now. The original design in the mid-1990s of the tropospheric ozone DIAL was optimized for tropospheric ozone and aerosol measurements (McDermid, 1991). The system was later re-designed to provide exclusively tropospheric ozone profiles (McDermid et al., 2002). The emitter uses a quadrupled Nd:YAG laser emitting two beams at 266 nm. One beam ~~is sent into~~passes through a Raman cell filled with Deuterium to shift the wavelength to 289 nm, the other beam ~~is sent into~~ passes through another cell filled with Hydrogen to shift the wavelength to 299 nm. The two beams are then expanded five times and transmitted into the atmosphere. The light elastically backscattered in the troposphere (3-20 km) is collected by

several <how many? 3?> telescopes comprising mirrors of diameters varying from 91 cm diameter to 5 cm diameter, thus accommodating for the large signal dynamic range ~~implied~~ occuring when collecting light from this close range. A total of three pairs of 289/299 nm channels is thus used to retrieve ozone using the DIAL technique, each pair corresponding to a different intensity range and the retrieved ozone profiles from all pairs combined ~~together~~ ultimately cover~~ing~~ the entire troposphere (3-18 km). As part of the retrieval process, the upper range of the ozone profile is further extended to about 25 km by applying the DIAL technique on the 299 nm high intensity channel of the tropospheric ozone lidar and the 355 nm low-intensity channel of the co-located water vapor Raman lidar (Leblanc et al., 2012).

The instrument temporal sampling can be set to any value from a few seconds to several hours, depending on the science or validation need. The vertical sampling can be set to any multiple of 7.5 m~~, again~~ depending on the science or validation need. For the routine measurements contributing to NDACC over the period 1999-2015 and used for the present work, the standard settings have typically ranged between 5-min and 20-min for temporal sampling, and between 7.5 m and 75 m for the vertical sampling. Profiles routinely archived at NDACC are averaged over 2-hours, with an effective vertical resolution varying from 150-m to 3 km, ~~depending on~~increasing with altitude. These temporal and vertical resolution settings yield a standard uncertainty of 7-14% throughout the profile. The system operates routinely at nighttime, but daytime measurements with reduced signal-to-noise ratio are occasionally performed in special circumstances such as process studies~~,~~ and aircraft or satellite validation. The total number of routine 2-hour ozone profiles used in this study and archived at NDACC for the period 2000-2015 is included in Table 1.

[Table 1]

The TMF ozone lidar measurements have been regularly validated using simultaneous, ~~and~~ co-located Electrochemical Concentration Cell (ECC) sonde measurements (Komhyr, 1969; Smit et al., 2007). In the troposphere the precision of the ozonesonde measurement is ~~around~~ approximately 3- 5% with accuracy of ???.~~-~~ TMF has ozonesonde launch capability since 2005 and 32 coincident profiles were obtained over the period 2005-2013. Results from the lidar and the ECC comparison are included in Figure 1. Figure 1c reveals that the deviations do not present significant changes with time, which is an indicator of the system stability despite the multiple upgrades made over this time

period. In most cases, differences were within ±15% for the complete analyzed period. Note that a non-negligible fraction of the differences is due to geophysical variability. The measurement geometry of the lidar and ozonesonde are radically different: 2-hour averaged, single location for lidar, and horizontally-drifting ~~instantaneous~~ 1-second measurements for the ozonesonde rising at 5 m/s.

2.2. Surface ozone measurements

Continuous surface ozone measurements have been performed at TMF since 2013 with a UV photometric ozone analyzer (Model 49i from Thermo Fisher Scientific, US). The operation principle is based on the absorption of UV light at 254 nm by the ozone molecules. The instrument collects in-situ air samples at 2 meter above ground taken from an undisturbed forested environment adjacent to the lidar building. It provides ozone mixing ratio values at 1-minute time intervals with a lower detection limit of 1 ppbv.

3. Results

3.1.Surface ozone variability

Figure 2a shows the surface ozone seasonal cycle at TMF and nearby stations from the California Air Resources Board (ARB) air-quality network for the period 2013-2015. The seasonal cycle at TMF comprises a maximum in spring and summer and a minimum in winter, consistent with the ARB stations shown, as well as other stations in the US West Coast (e.g. Schnell et al., 2015). Nonetheless, the seasonal cycle obtained at TMF from the hourly samples (left plot) presents larger ozone values and lower variability throughout the year compared to the other ARB stations all of which are lower altitudes. The mean surface value for the complete period at TMF is 55 ppbv, whereas the seasonal values are 57, 57, 52 and 45 ppbv in spring (March-April-May), summer (June-July- August), fall (September-October-November), and winter (December-January-February) respectively. These values are in good agreement with those obtained from surface measurements at high elevation sites in the Northern Hemisphere and reported in the review by Cooper et al., (2014). When using the 8hMDA (8-h maximum daily average, right plot), larger seasonal-cycle amplitudes ~~are observed~~occur, especially at stations affected by anthropogenic pollution such as Crestline or San Bernardino. These polluted stations present larger values in summer than those recorded at high-elevation remote stations like Joshua Tree or TMF. The

mean 8hMDA at TMF is 58 ppbv and the seasonal averages are 62, 66, 57 and 49 for spring, summer, fall and winter, respectively. The observed seasonal variability is typical of high-elevation remote sites with low urban influence (Brodin et al., 2010). A similar behavior can be observed at the Phelan, Joshua Tree or the Mojave National Preserve stations, all sites being at high elevation with low or negligible urban influence. In Figure 2a a secondary minimum is observed at TMF and most of the ARB nearby stations in July-August, followed by a secondary maximum in fall.

In Figure 2a a clear combined effect of the altitude and proximity to anthropogenic pollution sources on the ozone levels is observed. In general, higher ozone levels and lower variability are observed at higher altitudes. The lowest altitude Pico Rivera instrument measures the lowest ozone levels, and the highest-altitude TMF instrument measures the highest ozone levels throughout the year when considering the hourly sampled dataset. A mean difference of ~30 ppbv is observed for a 2-km altitude difference. The magnitude of this positive ozone vertical gradient depends on the distance from anthropogenic pollution sources. The effect of pollution is clearer on the 8hMDA data, where high-elevation stations, yet more likely to be affected by pollution such as Crestline or Victorville, present a larger seasonal cycle amplitude associated with lower ozone levels in winter and higher levels in summer. A similar impact of the interplay between urban and high-elevation was previously reported by Brodin et al., (2010).

The difference between the seasonal cycle retrieved from the 1-hour averaged data and the 8hMDA can be easily explained from the differences in the daily cycles at the different stations. The mean surface ozone diurnal cycle at TMF and nearby ARB stations is shown in Figure 2b for the four seasons. Minimum values are observed at nighttime, whereas maxima appear in late afternoon. As for the seasonal cycle, the daily cycle at TMF, Joshua Tree, Mojave National Preserve, and Phelan stations exhibit low variability compared to the other stations located at lower altitude and more affected by urban pollution. On average, daily values are larger at high-elevation remote sites such as TMF or Joshua Tree. However, the afternoon maximum is larger at polluted stations such as Crestline, especially in the summer season. In addition, the maximum at TMF and the ARB stations of Joshua Tree and Mojave National Preserve occurs later than at the other stations. The difference in timing is likely due to the different chemical species involved in the ozone formation and depletion processes due to the low influence of anthropogenic pollution

(Brodin et al., 2010; Gallardo et al., 2000; Naja et al., 2003). In winter, a minimum is observed at TMF in the afternoon instead of the maximum observed at the other stations. This difference in diurnal pattern has been observed at other remote or high-elevation sites and has been attributed to the shorter day length and the lack of ozone precursors compared to urban sites. The resulting daytime photochemical ozone formation is insufficient to produce an ozone diurnal variation maximizing in the afternoon (Brodin et al., 2010; Gallardo et al., 2000; Naja et al., 2003; Oltmans and Komhyr, 1986; Pochanart et al., 1999; Tsutsumi and Matsueda, 2000).

3.2.ropospheric ozone variability

The red curve in ~~Figure 3~~**Figure 3**a (left plot) shows the average tropospheric ozone profile obtained by the TMF lidar for the period 2000-2015. The cyan horizontal bars show the corresponding standard deviation at 1-km interval. The red dot at the bottom of the profile shows the 2013-2015 mean surface ozone obtained from the data acquired simultaneously to the lidar measurements. The lidar system ~~can~~ provides information from ~~around~~ approximately 3.5 km (from 200 meters since 2013) above the surface up to 25 km, covering the whole troposphere and the lower stratosphere. The average mixing ratio value in the mid-troposphere is 55 ppbv. Above 8 km, the ozone mixing ratio increases, reaching values above ~~1 ppmv~~100 ppbv at 16 km.

The seasonally averaged profiles are shown in Figure 3b. ~~They~~ These averages represent show larger values in spring and summer in the troposphere, whereas in the stratosphere maximum values ~~are observed~~ occurs in winter and spring. Within the troposphere, below 9 km, the seasonally-averaged profiles show average values of 62, 60, 51 and 50 ppbv in spring, summer, fall and winter respectively. These values are in good agreement with the average ozone concentrations (50-70 ppbv) obtained in previous studies (Thompson et al., 2007; Zhang et al., 2010) above the western U.S. In the altitude range 9-16 km (UTLS) a much larger variability in ozone is observed, as indicated by the large standard deviation (left plot) and the differences between the seasonally-averaged profiles (right plot). This large variability results from the horizontal and vertical displacement of the tropopause above the site, causing the lidar to sound either the ozone-rich lowermost stratosphere or the ozone-poor sub-tropical upper troposphere for a given altitude.

The 2D color contours of Figure 4 show the composite (2000-2015) monthly mean ozone climatology measured by lidar (main panel, 4-20 km). A similar 2D color contour representation

was used just below the main panel to represent the composite (2013-2015) monthly mean surface ozone. The climatological tropopause height at TMF is also included in the main panel (blue dotted line), with mean values ranging between 12 and 15 km. As will be discussed later in this paper, the tropopause height variability is the main cause of the larger standard deviation observed in Figure 3a in this region. Between the surface and 9 km, a very consistent seasonal pattern ~~is observed~~occurs, with maximum values in April-May and minimum values in winter. The spring-summer maximum in the free-troposphere has been consistently observed at other stations in Europe and North America and is attributed to photochemical production (Law et al., 2000; Petetin et al., 2015; Zbinden et al., 2006). Above 9 km, the seasonal maximum ~~is observed~~ occurs earlier~~,~~ (i.e., in March and April between 10 and 12 km and February and March at higher altitudes~~),~~ consistent with the transition towards a dynamically-driven lower-~~-~~stratospheric regime. At these altitudes, the ozone minimum is also displaced earlier in the year (August-October), which is consistent with the findings of Rao et al. (2003) above Europe.

The TMF surface and lidar data are found to be very consistent, both in terms of seasonal cycle phase and amplitude, and in term of absolute mixing-~~-~~ratio values. The mean value obtained from the lidar measurements in the troposphere is very similar to the mean value obtained from the surface measurements (around 55 ppbv). This consistency may point out the fact that the TMF surface measurements are representative of the lower part of the free troposphere (i.e., below 7 km), at least during the nighttime lidar measurements.

The consistency between the lidar and the surface data was found not only for the seasonal cycle obtained from the monthly averaged values, but also for the complete time series. The degree of correlation between the lidar measurements at the lowest point and the surface measurements was investigated. ~~As mentioned before,~~Although the lidar cannot measure all the way down to the surface., ~~T~~the first valid measurement occurs at ~~around~~ 3.5-4 km depending on the time period. Therefore, the layer from 4 to 6 km is considered as the lower lidar layer. A correlation coefficient of R=0.34 was found between the lidar data in the layer from 4 to 6 km and the surface data. The correlation increases somewhat (R=0.44) if we consider a 3-hour time lag between the 4-6 km layer and the surface. After removing outliers <not legitimate here> corresponding to ozone values higher (or lower) than the average plus (minus) one standard deviation either at the surface or at 4-6 km, the correlation increases up to 0.69 for the simultaneous data and up to 0.79 for the 3-hour time- shift.

Formatted: Highlight

3.3. Interannual variability and trends

The 2000-2015 time-series of the deseasonalized ozone mixing ratio is shown in Figure 5. Anomalies, expressed in percent~~, were calculated~~ resulted from~~ by~~ subtracting the climatological ozone monthly mean profiles computed for the period 2000-2015 ~~to~~ from the measured lidar profiles. Large ozone variability with time is clearly observed, highlighting the difficulty ~~to~~ in identifying~~y~~ trends and patterns. No clear mode of interannual variability is observed for the analyzed period here. However, positive anomalies seem to predominate throughout the troposphere during the period 2003-2007, especially below 7 km. On average, ozone mixing ratio values in the lower troposphere were 5 ppbv larger in 2003-2007 than during the entire period 2000-2015.

Following a procedure similar to that described in Cooper et al. (2012), a trend analysis was performed at different altitude levels (Table 2 and Figure 6). Figure 6 shows the time series of the median, 95th and 5th percentile values, obtained every year between 2000 and 2015 for different layers and different seasons using the lidar profiles measured at TMF. ~~In order to obtain the trends, l~~Linear fits (shown in Figure 6) of the median, 95th and 5th percentiles ~~were performed~~ independently using the least squares method define the trend lines of~~. T~~the ozone rate of change in ppbv.year^{-1} ~~was determined from the slope of the linear fit.~~ To assess the significance of the trends, the F-statistic test was used, with the p-Value as an indicator of the statistical significance. ~~For p~~P-Values lower than 0.1 <Suggest you use 0.05>~~,~~ indicate trends ~~were assumed~~ statistically significant, with a confidence level larger than 9~~0~~5%.

Formatted: Right: 0", Space Before: 0 pt, Line spacing: Exactly 14.35 pt

The calculated trends ~~were found to~~ depend on altitude and season. Table 2 contains the ozone rate change expressed in ppbv.year^{-1} (and %.year^{-1}) for the different layers and seasons for the median, 5th and 95th percentiles. Statistically significant trends are marked in bold font. The layer corresponding to the upper troposphere (7-10 km) shows a statistically significant ozone increase of 0.31 ppbv.year^{-1} (0.57%·year^{-1}) for the median values and 0.55 ppbv.year^{-1} (0.54%.year^{-1}) for the 95th percentile, indicating that both the background and the high~~-~~ intensity ~~events~~ ozone-event ~~-~~levels were increasing (Cooper et al., 2012, 2014). Cooper et al. (2012) ~~A~~a similar increase in the free troposphere and in the western US ~~was reported by Cooper et al. (2012)~~ for the period 1990-2010 for both the median and 95th percentiles.

~~Now looking at~~Analyzing each season separately, a significant positive trend ~~was found~~ occurs in the upper troposphere (7-10 km) for both spring and summer, with an ozone

increasing rate of 0.71

and 0.58 ppbv.year^{-1} respectively (or 1.10 and 0.98%·year^{-1}), and an ozone decrease of -0.43 ppbv.year^{-1} (-0.87%·year^{-1}) during winter. Whereas a positive trend was obtained on a regional scale in Cooper et al., (2012) for winter, certain sites in the western U.S. showed ~~a~~ negative trends. The positive trend ~~obtained here~~ at TMF in spring for the median values is larger than the trend

obtained by Cooper et al. (2012) for the free troposphere in 1995-2011 (0.41 ppbv.year^{-1}), and even larger than the trend obtained by Lin et al. (2015b) using model ~~data~~calculations (0.37 ppbv.year^{-1} during 1995-2012). This disagreement could be due to differences in sampling, as concluded in Lin et al. (2015b). Nonetheless, Figure 6 shows larger ozone median (and 5th and 95th percentile) values at 7-10 km in 2013-2015 than in preceding years, with this period ~~not~~ being ~~in~~excluded in the previous studies. A lower ozone increasing rate in 2000-2012 above TMF (0.43 ppbv.year^{-1}) suggests that that the ozone rate of change has increased in the last years, but a more comprehensive study with regional coverage would be necessary to confirm the significance of this change.

Statistically significant trends were also found in the lower troposphere (4-7 km) during winter for the median and 5th percentile values with an ozone decrease of -0.36 ppbv.year^{-1} and -0.59 ppbv.year^{-1} , ~~r~~respectively (-0.72% and -1.53%·year^{-1} ~~respectively~~) (Table 2). ~~This~~ These trends indicate~~s~~ a decrease in the background ozone values. During winter months, a smaller influence of transboundary~~-~~ ~~–~~ozone transport is expected at low altitudes above TMF and the decrease in background ozone during these months could be associated with the decrease in domestic anthropogenic emissions.

~~No significant t~~Trend ~~was observed~~ near the tropopause (12-16 km) are not significant;~~-~~ whereas a significant negative trend of -8.8~~79~~ ppbv.year^{-1} (-1.3~~94~~%·year^{-1}) for the median and -5.8~~0~~ ppbv.year^{-1} (- 1.2~~63~~%·year^{-1}) for the 5th percentile in fall ~~was observed~~occured in the lower stratosphere (17-19 km).

3.4. Characterization of the air masses sounded by the TMF tropospheric ozone lidar

In an attempt to characterize the air parcels sounded by lidar above TMF based on their travel history, 8-day backward trajectories ending at TMF between 5 and 14 km altitude were computed using the HYSPLIT4 model (Draxler and Rolph, 2003), http://www.arl.noaa.gov/ready/hysplit4.html). The NCAR/NCEP Reanalysis Pressure level data were used as meteorological input (Kalnay and Kanamitsu, 1996) in HYSPLIT4. These data, available since 1948, provide 4-times-daily meteorological information at 17 pressure levels

between the 1000 and 10 hPa and 2.5x2.5 degrees horizontal resolution. Several studies (Harris et al., 2005; Stohl, 1998) provided a wide range of uncertainty estimates along the trajectories. The more recent study by Engström and Magnusson, (2009) indicate values of 354-400 km before 4 days and 600 km after.

<What does this last sentence mean?>

Our trajectory analysis comprises two steps. First, the 8-day backward trajectories computed by HYSPLIT and ending at different altitude levels were grouped using the HYSPLIT clustering tool (Draxler et al., 2009) in order to identify the most significant paths followed by the air masses arriving over the station. Based on the results of this preliminary analysis, five main regions were identified: the stratosphere, the Asian boundary layer (ABL), the free-troposphere above Asia (AFT), Central America, and the Pacific Ocean. Once these geographical areas were identified, we performed a classification of the air parcels according to the criteria described next.

An air parcel was classified as "stratospheric" if the 8-day backward trajectory intercepted the tropopause and resided at least 2 days above the local tropopause. The tropopause height information comes from the global tropopause height data derived once a day by the NOAA Physical Sciences Division (http://www.esrl.noaa.gov/psd) from the same NCAR/NCEP Reanalysis database used as input to HYSPLIT4. Computations are based on the World Meteorological Organization (WMO, 1957) definition, that is, the lowest height at which the temperature lapse rate becomes lower than 2 $K.km^{-1}$, provided that along 2 km above this height the average lapse is also lower than 2 $K.km^{-1}$. In addition, the NOAA computations do not allow tropopause heights at pressure levels larger than 450 hPa and smaller than 85 hPa.

Next, the air parcels that were not classified as "stratosphere" were then classified as "Asian boundary layer" (ABL) for trajectories comprising a minimum residence time of 2 days within the area labelled "ABL" in Figure7, and below an altitude of 3 km. Next, air parcels with trajectories comprising a minimum residence time of 2 days within the area labelled "AFT" in Figure7, and above 3 km altitude were classified as "Asian Free-troposphere" (AFT).

The air parcels not classified as "stratosphere", "ABL", or "AFT" were then classified as "Central America" if the corresponding trajectories' residence time over the "Central America" region depicted in Figure7 was found to be at least 2 days. Finally, the remaining parcels were

366 classified as “Pacific Ocean” when the residence time above the corresponding region (see figure
367 7) reached or exceeded 2 days.

368 The classification of the air parcels took place sequentially, which means that each
369 category is exclusive of the others. The classification was made for each of the four seasons
370 separately in order to account for the seasonal changes in synoptic circulation. Examples of the
371 corresponding classified back-trajectories are shown in Figure 8. The number and frequency of
372 occurrences of each air parcel category for all seasons is compiled in Table 3. A monthly
373 distribution of these occurrences is shown in Figure 9. With the selection criteria we have set, a
374 very low number of parcels classified “ABL” were found. Air parcels dominantly originate in the
375 Pacific Ocean below 10 km, with almost equal influence throughout the year. Increasing
376 influence of the stratosphere is observed at upper levels, with values ranging between 2 to 78%
377 or higher during winter and spring. This result agrees well with previous studies in the Western
378 US (Sprenger, 2003; Stohl, 2003). A statistically significant Central American influence was
379 identified in summer with a frequency of the occurrence varying between 11% and 3%,
380 decreasing with altitude. The Central America influence coincides with the establishment of the
381 North American Monsoon circulation from July to September and which affects Central America
382 and the Southwestern US.

383 Composite ozone profiles were estimated for each category of air parcel and for altitudes
384 between 4.5 and 13.5 km at 1-km altitude intervals. Figure 10 shows the ozone mixing ratio
385 mean (open circles), median (red bars), 25^{th} and 75^{th} percentiles (blue bars) at 9 km altitude for
386 each of the identified categories and season. The number of occurrences for each category is
387 mentioned between parentheses. The ozone statistics obtained when a low number of
388 occurrences was found should be ignored (e.g., Central America in Spring, or ABL for most
389 seasons). Figure 11 shows, for each season, the composite ozone profiles constructed from the
390 ozone mixing ratio median values found for a particular category at a given altitude. In order to
391 keep the most statistically significant results, composite values computed using less than 5% of
392 the total number of samples for a given season were not plotted, leaving out certain sections of
393 the composite profiles, and in the case of ABL, leaving out the entire profile.

394 Not surprisingly, the analysis reveals that larger ozone mixing ratio values were observed
395 when the air masses were classified as “stratospheric” regardless of altitude and season (65-85

ppbv below 9 km). For this category, large ozone variability was found, as indicated by the 25th and 75th percentiles in Figure 10. As altitude increases, the influence of the stratosphere is more important, exceeding 30% above 12 km, resulting in higher ozone mixing ratio values (red curves in Figure 11).

Conversely, low ozone mixing ratio values (50-65 ppbv below 9 km) were consistently associated with the air parcels classified as "Pacific Ocean" (cyan curves). This region can be considered as a source of 'background ozone', since no anthropogenic source is expected to affect the local ozone budget. Slightly higher ozone content (50-70 ppbv higher) is systematically found for air parcels classified as "Asian free-troposphere" (AFT), but the number of occurrences remains too small to provide any meaningful interpretation. No conclusion can be made for air parcels classified as "Asian Boundary layer" (ABL) due to the very low number of occurrences found.

During summer, ozone values of about 70 ppbv were found at 9 km altitude for the 85 air parcels classified as "Central America" (yellow curve). The corresponding values for the 277 air parcels classified as "Pacific Ocean" are about 55 ppbv, which is 15 ppbv lower. This difference possibly points out to the lightning-induced enhancement of ozone within the more frequent occurrence of thunderstorms during the North American summer monsoon.

3.5. The influence of tropopause folds on the TMF tropospheric ozone record

In the previous section, a large variability in the composite ozone content was found for the air parcels classified as "stratospheric". In the current section, we provide at least one clear explanation for this large variability. Tropopause folds are found primarily in the vicinity of the subtropical jets, in the 20º-50º latitude range. They typically consist of three-dimensional folds of the virtual surface separating air masses of tropospheric characteristics (weakly stratified, moist, low ozone concentration, etc.) and those of stratospheric characteristics (highly stratified, dry, high ozone concentration, etc.). Tropopause folds can result in the transport of large amounts of stratospheric ozone into the troposphere, reaching in some cases the planetary boundary layer and enhancing ozone amounts even at the surface (Chung and Dann, 1985; Langford et al., 2012; Lefohn et al., 2012; Lin et al., 2012a). They are considered one of the main mechanisms of stratosphere-to-troposphere exchange and have been widely studied in the past (e.g. Bonasoni

and Evangelisti, 2000; Danielsen and Mohnen, 1977; Lefohn et al., 2011; Vaughan et al., 1994; Yates et al., 2013). Due to the location of TMF, the upper troposphere above the site is frequently impacted by tropopause folds. The MERRA reanalysis (1-km vertical resolution, 1 x 1.25 degrees horizontal resolution) were used in this study to identify the presence of double tropopauses above the station. A comparison between the MERRA temperature profiles and the temperature profiles measured by the radiosondes launched at TMF was performed in order to evaluate the performance of MERRA above TMF. The comparison (not shown) reveals excellent agreement, with average relative differences of 2% or less from the surface up to 25 km. The heights of double tropopauses were computed following a methodology similar to that proposed in Chen et al., (2011). The first (lower) tropopause is identified according to the WMO definition, as explained earlier. A second (upper) tropopause is identified above the WMO tropopause if the temperature lapse rate increases over 3 K/km within at least 1 km, and its height is determined once again by the WMO criterion.

Using this methodology, we found that 27% of the TMF tropospheric ozone lidar profiles were measured in the presence of double tropopauses. Figure 12 shows the number of cases with double tropopauses above TMF distributed per months, with the number of days with tropopause folds being normalized to the total number of measurements every month (compiled in Table 1). As we can see, the presence of double tropopauses was especially frequent during winter and spring, which coincides with the higher frequency of stratospheric air masses arriving at TMF estimated by the backward trajectories analysis (Figure 9). The altitude of detected single tropopauses is found around 13 km in winter and spring, and 16-17 km in summer and fall (Figure 13a-d). When a double tropopause is identified, the altitude of the lower tropopause ranges between 8 and 15 km, with the distribution peak centered around 12-13 km (Figure 13e-h), and the second tropopause is detected typically around 17-18 km (Figure 13i-l).

Figure 14 shows the average of all tropospheric ozone lidar profiles measured in winter (blue curves) and spring (red curves) in the presence of a double tropopause (solid curves), and in the presence of a single tropopause (dashed curves). The right panel (Figure 14b) is simply a lower tropospheric-zoomed version of the left panel (Figure 14a). Only winter and spring are shown because they are the seasons most affected by double tropopause cases as previously stated. In the presence of double tropopauses a clear dual vertical structure in ozone is observed,

with higher ozone values between 9 and 14 km and lower mixing ratio values between 14 and 18 km. This dual structure is consistent with the expected origin of the air masses within a tropopause fold. Stratospheric air, richer in ozone, is measured within the lower half of the fold (12-14 km), while tropospheric ozone-poor air is measured within the upper half of the fold (14-18 km). In the case of deep stratospheric intrusions, ozone-rich stratospheric air masses embedded in the lower half of the fold can reach lower altitudes, and occasionally the planetary boundary layer mixing down to the surface (Chung and Dann, 1985; Langford et al., 2012, 2015; Lefohn et al., 2012; Lin et al., 2012a), leading to an ozone increase in the lower troposphere (Figure 14b). In our case, the mean increase is around 2 ppbv below 6 km for both spring and winter. Note the relative magnitude of the ozone anomalies in the lower and upper halves of the fold is different for spring and winter. A detailed investigation, beyond the scope of the present work, is needed to assess the actual significance of this difference.

4. Summary and discussion

Long-term (2000-2015) tropospheric ozone measurements obtained from the differential absorption lidar located at the JPL Table Mountain Facility in Southern California (elev. 2285 m) were used for the first time to investigate ozone variability at time-scales ranging from days to decades. The routine nighttime lidar profiles (3.5-25 km) were complemented by 24-hour continuous surface ozone measurements acquired since 2013. The present study allowed the characterization of the full profile from the ground to the stratosphere, and is particularly valuable in the context of a notoriously sparse horizontal coverage for this type of vertically resolved measurements in a region affected by transboundary ozone inflow and stratospheric intrusions.

The observed diurnal and seasonal variability is consistent with that observed at other high-elevation rural sites, implying high values and low amplitudes of the seasonal and diurnal cycles compared to those observed at low elevation and/or urban sites (Brodin et al., 2010; Gallardo et al., 2000; Naja et al., 2003). The monthly mean surface ozone mixing ratio agrees well with that measured by lidar in the lower troposphere throughout the year (Figure 4), thus revealing that nighttime surface conditions are representative of nighttime lower tropospheric conditions. Additional daytime lidar measurements will be performed in 2016 to assess whether such consistency also exists at other times of the day, especially in the afternoon.

The analysis of the long-term lidar time-series (16 years covered) shows no significant signatures of interannual variability, though larger ozone values were generally observed in 2003-2007 compared to the rest of the measurement period. More importantly, no obvious signature of ENSO or the QBO could be identified, which is inconsistent with the recent findings of Lin et al., (2015) or Neu et al., (2014), who have linked tropospheric ozone variability in the Northern Hemisphere to El Niño/ La Niña events, and the QBO, through the variations of stratospheric/tropospheric ozone fluxes. However, this inconsistency might not be so surprising if we take into account the obvious difference in measurement sampling (one single location in the Western U.S. as opposed to global observations). Nevertheless, our analysis reveals statistically-significant trends for selected seasons and altitudes. Specifically, a positive trend of 0.31 ppbv.year^{-1} (ozone annual median) was found in the upper troposphere (7-10 km). This positive trend is more pronounced in spring and summer (0.71 and 0.58 ppbv.year^{-1} respectively), whereas a negative trend (-0.43 ppbv.year^{-1}) was found in winter. A negative trend of -0.36 ppbv.year^{-1} was also detected in winter in the lower troposphere (4-7 km). <These results should include trend uncertainties and should include only significant figures in the trend estimates. The wintertime negative results require an explanation.> Our springtime positive trend estimates only broadly agree with those reported in the literature. The two-decade-long efforts to implement regulations to control air quality and anthropogenic emissions in the U.S. have led to a clear decrease in ozone levels in the Eastern U.S., but not in the Western U.S. (e.g. Copper et al., 2012; 2014). This different regional behavior has been attributed to the inflow of elevated ozone, mainly from East Asia, and to the increasing contribution of stratospheric intrusions (Cooper et al., 2010; Jacob et al., 1999; Parrish et al., 2009; Reidmiller et al., 2009). But again, differences in sampling can impact significantly the interpretation of our trend estimates. As pointed out by Lin et al. (2015b), further coordination efforts at both global and regional scales are necessary in order to reduce biases introduced by inhomogeneity in sampling. As part of these efforts, an extended analysis based on the origin of the air masses sampled by the TMF lidar is under way, with the ultimate objective to filter out synoptic noise ~~out~~, and better quantify the ENSO and QBO signals and the residual trends. As a prerequisite to such study, a preliminary characterization of the air masses sounded by the TMF lidar was performed and presented here.

Backward trajectories were computed in an attempt to classify the air masses sampled by the TMF lidar over the period 2000-2015. Our classification, based on a 2-day <Perhaps too long a requirement?> residence time within each region, comprised five categories, namely "stratosphere", 'Pacific Ocean", "Asian

Boundary Layer", "Asian free-troposphere", and "Central America". After computing more than 20,000 8-day back-trajectories covering the troposphere every 1–km for each lidar measurement made between 2000 and 2015, the Pacific Ocean and the stratosphere categories were found most frequently. Not surprisingly, parcels identified as "stratosphere" contain the highest ozone mixing ratios, and parcels classified as "Pacific Ocean" contain the lowest ozone concentrations, which can be considered as 'background conditions'. No outstanding signature from the Asian boundary layer could be identified due to the low number occurrences associated with this category. Nevertheless, air parcels classified as "Asian free-troposphere" seemed to contain systematically more ozone than those classified as "Pacific Ocean", especially below 9 km. A refined classification, probably requiring the use of chemistry-transport models, is needed to assess whether the Asian boundary layer or the Asian free-troposphere have a detectable impact on the ozone content measured above TMF.

In summer, air masses coming from Central America were frequently detected. The ozone mixing ratio values measured in this case were clearly above the climatological mean, with values up to 15 ppbv larger than those associated with the Pacific Ocean region. Previous studies (Cooper et al., 2009), have observed enhanced ozone values associated with the North American Monsoon, mainly due to ozone production associated with lightning (Choi et al., 2009; Cooper et al., 2009). However, this feature was observed in the Eastern U.S. Because of the synoptic conditions during the monsoon, the Western U.S. is not as much influenced and no significant ozone increase was reported (Barth et al., 2012; Cooper et al., 2009). Nevertheless, Cooper et al., (2009) reported higher modeled lightning-induced NO_x concentrations at TMF than at other western locations, which would be consistent with our findings. Further investigation, including a detailed history of the meteorological conditions along the trajectories, is needed to confirm this correlation.

As part of the characterization of the TMF lidar-sampled air masses, the impact of double tropopauses was assessed. The presence of a double tropopause was identified using the MERRA temperature profiles interpolated at the location of TMF. Between 2000 and 2015, the frequency of occurrence of double tropopauses above TMF was found to be around 27%. This high frequency, especially observed in winter and spring, was expected considering the latitude of TMF, i.e., near the subtropical jet, where frequent tropopause folds occur. More interestingly, a

clear, dual vertical structure in ozone was observed in the presence of a double tropopause (Figure 14). The first (lower) tropopause, which typically coincides with the WMO tropopause reported by meteorological services, was systematically identified around 12-14 km. The second (upper) tropopause was mostly identified around 15-18 km. The double tropopause is expected to result from a tropopause fold in the layer between the two identified tropopauses. The dual ozone structure observed by lidar coincides with the expected location of the fold, and consists of systematically higher-than-average mixing ratios in the lower half of the fold (12-14 km), and lower-than-average mixing ratios in the upper half of the fold (14-18 km). In addition, statistically significant higher-than-average mixing ratios (+2 ppbv) are observed in the lower troposphere (4-10 km) in the presence of double-tropopauses. This increase is consistent with previous reports of the importance of the stratosphere as an ozone source in the lower troposphere (Cooper and Stohl, 2005; Langford et al., 2012; Lefohn et al., 2011; Trickl et al., 2011), with a 25 to 50% contribution to the tropospheric budget (Davies and Schuepbach, 1994; Ladstätter-Weißenmayer et al., 2004; Roelofs and Lelieveld, 1997; Stevenson et al., 2006).

Further investigation is now underway, with the objective of better identifying all signatures of interannual variability and trends. This long-term variability investigation not only will include an air mass classification based on geographical area, but will also take into account the history of the air parcels in the context of nearby tropopause folds. Altogether, this air parcel characterization, used in conjunction with regional chemistry-climate or chemistry-transport model runs, should unveil signatures hidden in the current lidar record, and eventually shed new light on the origin of the reported past, current, and future tropospheric ozone trends over the Western U.S.

ACKNOWLEDGEMENTS

The work described in this paper was carried out at the Jet Propulsion Laboratory, California Institute of Technology, under a Caltech Postdoctoral Fellowship sponsored by the NASA Tropospheric Chemistry Program. Support for the lidar, surface, and ozonesonde measurements was provided by the NASA Upper Atmosphere Research Program. The authors would like to thank M. Brewer, T. Grigsby, J. Howe, and members of the JPL Lidar Team who assisted in the collection of the data used here. The authors gratefully acknowledge the NOAA Air Resources Laboratory (ARL) for the provision of the HYSPLIT transport and dispersion

model and/or READY website (http://www.ready.noaa.gov) and the NCEP/NCAR Reanalysis team for the data used in this publication. We would also like to thank Dr. Susan Strahan and the MERRA Reanalysis team for providing the data used in this study and to acknowledge the California Air Resources Board for providing the surface ozone data.

REFERENCES

Ambrose, J., Reidmiller, D. and Jaffe, D.: Causes of high O 3 in the lower free troposphere over the Pacific Northwest as observed at the Mt. Bachelor Observatory, Atmos. Environ., 2011.

Barth, M. C., Lee, J., Hodzic, A., Pfister, G., Skamarock, W. C., Worden, J., Wong, J. and Noone, D.: Thunderstorms and upper troposphere chemistry during the early stages of the 2006 North American Monsoon, Atmos. Chem. Phys., 12(22), 11003–11026, doi:10.5194/acp-12-11003-2012, 2012.

Bonasoni, P. and Evangelisti, F.: Stratospheric ozone intrusion episodes recorded at Mt. Cimone during the VOTALP project: case studies, Atmos. …, 2000.

Brodin, M., Helmig, D. and Oltmans, S.: Seasonal ozone behavior along an elevation gradient in the Colorado Front Range Mountains, Atmos. Environ., 44(39), 5305–5315, doi:10.1016/j.atmosenv.2010.06.033, 2010.

Brown-Steiner, B. and Hess, P.: Asian influence on surface ozone in the United States: A comparison of chemistry, seasonality, and transport mechanisms, J. Geophys. Res. Atmos., 116(17), 1–13, doi:10.1029/2011JD015846, 2011.

Bufton, J. L., Stewart, R. W. and Weng, C.: Remote measurement of tropospheric ozone., Appl. Opt., 18(20), 3363–4, doi:10.1364/AO.18.003363, 1979.

Choi, Y., Kim, J., Eldering, A., Osterman, G., Yung, Y. L., Gu, Y. and Liou, K. N.: Lightning and anthropogenic NOx sources over the United States and the western North Atlantic Ocean: Impact on OLR and radiative effects, Geophys. Res. Lett., 36(17), L17806, doi:10.1029/2009GL039381, 2009.

Chung, Y. and Dann, T.: Observations of stratospheric ozone at the ground level in Regina, Canada, Atmos. Environ., 1985.

Cooper, O. and Stohl, A.: A springtime comparison of tropospheric ozone and transport pathways on the east and west coasts of the United States, J. …, 2005.

Cooper, O. R., Forster, C., Parrish, D., Trainer, M., Dunlea, E., Ryerson, T., Hübler, G., Fehsenfeld, F., Nicks, D., Holloway, J., de Gouw, J., Warneke, C., Roberts, J. M., Flocke, F. and Moody, J.: A case study of transpacific warm conveyor belt transport: Influence of merging airstreams on trace gas import to North America, J. Geophys. Res. Atmos., 109(D23), n/a–n/a, doi:10.1029/2003JD003624, 2004.

Cooper, O. R., Eckhardt, S., Crawford, J. H., Brown, C. C., Cohen, R. C., Bertram, T. H., Wooldridge, P., Perring, A., Brune, W. H., Ren, X., Brunner, D. and Baughcum, S. L.: Summertime buildup and decay of lightning NO_x and aged thunderstorm outflow above North America, J. Geophys. Res., 114(D1), D01101, doi:10.1029/2008JD010293, 2009.

Cooper, O. R., Parrish, D. D., Stohl, A., Trainer, M., Nédélec, P., Thouret, V., Cammas, J. P., Oltmans, S. J.,

613 Johnson, B. J., Tarasick, D., Leblanc, T., McDermid, I. S., Jaffe, D., Gao, R., Stith, J., Ryerson, T., Aikin, K.,
614 Campos, T., Weinheimer, A. and Avery, M. A.: Increasing springtime ozone mixing ratios in the free
615 troposphere over western North America, Nature, 463(7279), 344–348, doi:10.1038/nature08708, 2010.

616 Cooper, O. R., Gao, R.-S., Tarasick, D., Leblanc, T. and Sweeney, C.: Long-term ozone trends at rural
617 ozone monitoring sites across the United States, 1990-2010, J. Geophys. Res. Atmos., 117(D22), n/a–n/a,
618 doi:10.1029/2012JD018261, 2012.

619 Cooper, O. R., Parrish, D. D., Ziemke, J., Balashov, N. V., Cupeiro, M., Galbally, I. E., Gilge, S., Horowitz, L.,
620 Jensen, N. R., Lamarque, J.-F., Naik, V., Oltmans, S. J., Schwab, J., Shindell, D. T., Thompson, A. M.,
621 Thouret, V., Wang, Y. and Zbinden, R. M.: Global distribution and trends of tropospheric ozone: An
622 observation-based review, Elem. Sci. Anthr., 2, 000029, doi:10.12952/journal.elementa.000029, 2014.

623 Cui, J., Sprenger, M., Staehelin, J., Siegrist, A., Kunz, M., Henne, S. and Steinbacher, M.: Impact of
624 stratospheric intrusions and intercontinental transport on ozone at Jungfraujoch in 2005: comparison
625 and validation of two Lagrangian approaches, Atmos. Chem. Phys., 9(10), 3371–3383, doi:10.5194/acp-
626 9-3371-2009, 2009.

627 Danielsen, E. F. and Mohnen, V. A.: Project dustorm report: ozone transport, in situ measurements, and
628 meteorological analyses of tropopause folding, J. Geophys. Res., 82(37), 5867–5877,
629 doi:10.1029/JC082i037p05867, 1977.

630 Davies, T. D. and Schuepbach, E.: Episodes of high ozone concentrations at the earth's surface resulting
631 from transport down from the upper troposphere/lower stratosphere: a review and case studies,
632 Atmos. Environ., 28(1), 53–68, doi:10.1016/1352-2310(94)90022-1, 1994.

633 Derwent, R. G., Simmonds, P. G., Manning, A. J. and Spain, T. G.: Trends over a 20-year period from 1987
634 to 2007 in surface ozone at the atmospheric research station, Mace Head, Ireland, Atmos. Environ.,
635 41(39), 9091–9098, doi:10.1016/j.atmosenv.2007.08.008, 2007.

636 Draxler, R., Stunder, B., Rolph, G. and Taylor, A.: Hysplit 4 User's Guide, NOAA Air Resources Laboratory,
637 Silver Spring, 2009.

638 Dufour, G., Eremenko, M., Orphal, J. and Flaud, J.-M.: IASI observations of seasonal and day-to-day
639 variations of tropospheric ozone over three highly populated areas of China: Beijing, Shanghai, and Hong
640 Kong, Atmos. Chem. Phys., 10(8), 3787–3801, doi:10.5194/acp-10-3787-2010, 2010.

641 Feister, U. and Warmbt, W.: Long-term measurements of surface ozone in the German Democratic
642 Republic, J. Atmos. Chem., 5(1), 1–21, doi:10.1007/BF00192500, 1987.

643 Forster, P., Ramaswamy, V., Artaxo, P., Bernstsen, T., Betts, R., Fahey, D. W., Haywood, J., Lean, J., Lowe,
644 D. W., Myhre, G., Nganga, J., Prinn, R., Raga, G., Schulz, M. and Van Dorland, R.: Changes in atmospheric
645 constituents and in radiative forcing. Chapter 2, Cambridge University Press, Cambridge, United
646 Kingdom and New York, NY, USA., 2007.

647 Gallardo, L., Carrasco, J. and Olivares, G.: An analysis of ozone measurements at Cerro Tololo (30
648 degrees S, 70 degrees W, 2200 m.a.s.l.) in Chile, Tellus Ser. B-Chemical Phys. Meteorol., 52(1), 50–59,
649 doi:10.1034/j.1600-0889.2000.00959.x, 2000.

650 Gao, J., Wang, T., Ding, A. and Liu, C.: Observational study of ozone and carbon monoxide at the summit
651 of mount Tai (1534m a.s.l.) in central-eastern China, Atmos. Environ., 39(26), 4779–4791,
652 doi:10.1016/j.atmosenv.2005.04.030, 2005.

653 Granier, C., Bessagnet, B., Bond, T., D'Angiola, A., Denier van der Gon, H., Frost, G. J., Heil, A., Kaiser, J.

W., Kinne, S., Klimont, Z., Kloster, S., Lamarque, J.-F., Liousse, C., Masui, T., Meleux, F., Mieville, A., Ohara, T., Raut, J.-C., Riahi, K., Schultz, M. G., Smith, S. J., Thompson, A., van Aardenne, J., van der Werf, G. R. and van Vuuren, D. P.: Evolution of anthropogenic and biomass burning emissions of air pollutants at global and regional scales during the 1980–2010 period, Clim. Change, 109(1-2), 163–190, doi:10.1007/s10584-011-0154-1, 2011.

Jacob, D. J., Logan, J. A. and Murti, P. P.: Effect of rising Asian emissions on surface ozone in the United States, Geophys. Res. Lett., 26(14), 2175–2178, doi:10.1029/1999GL900450, 1999.

Jaffe, D., Bertschi, I., Jaeglé, L., Novelli, P., Reid, J. S., Tanimoto, H., Vingarzan, R. and Westphal, D. L.: Long-range transport of Siberian biomass burning emissions and impact on surface ozone in western North America, Geophys. Res. Lett., 31(16), L16106, doi:10.1029/2004GL020093, 2004.

Ladstätter-Weißenmayer, A., Meyer-Arnek, J., Schlemm, A. and Burrows, J. P.: Influence of stratospheric airmasses on tropospheric vertical O_3 columns based on GOME (Global Ozone Monitoring Experiment) measurements and backtrajectory calculation over the Pacific, Atmos. Chem. Phys., 4(4), 903–909, doi:10.5194/acp-4-903-2004, 2004.

Langford, A. O., Brioude, J., Cooper, O. R., Senff, C. J., Alvarez, R. J., Hardesty, R. M., Johnson, B. J. and Oltmans, S. J.: Stratospheric influence on surface ozone in the Los Angeles area during late spring and early summer of 2010, J. Geophys. Res. Atmos., 117(D21), n/a–n/a, doi:10.1029/2011JD016766, 2012.

Langford, A. O., Pierce, R. B. and Schultz, P. J.: Stratospheric intrusions, the Santa Ana winds, and wildland fires in Southern California, Geophys. Res. Lett., n/a–n/a, doi:10.1002/2015GL064964, 2015.

Law, K. S., Plantevin, P.-H., Thouret, V., Marenco, A., Asman, W. A. H., Lawrence, M., Crutzen, P. J., Muller, J.-F., Hauglustaine, D. A. and Kanakidou, M.: Comparison between global chemistry transport model results and Measurement of Ozone and Water Vapor by Airbus In-Service Aircraft (MOZAIC) data, J. Geophys. Res., 105(D1), 1503, doi:10.1029/1999JD900474, 2000.

Leblanc, T., McDermid, I. S. and Walsh, T. D.: Ground-based water vapor raman lidar measurements up to the upper troposphere and lower stratosphere for long-term monitoring, Atmos. Meas. Tech., 5(1), 17–36, doi:10.5194/amt-5-17-2012, 2012.

Lee, S. and Akimoto, H.: Lower tropospheric ozone trend observed in 1989–1997 at Okinawa, Japan, Geophys. …, 25(10), 1998, 1998.

Lefohn, A. S., Wernli, H., Shadwick, D., Limbach, S., Oltmans, S. J. and Shapiro, M.: The importance of stratospheric–tropospheric transport in affecting surface ozone concentrations in the western and northern tier of the United States, Atmos. Environ., 45(28), 4845–4857, doi:10.1016/j.atmosenv.2011.06.014, 2011.

Lefohn, A. S., Wernli, H., Shadwick, D., Oltmans, S. J. and Shapiro, M.: Quantifying the importance of stratospheric-tropospheric transport on surface ozone concentrations at high- and low-elevation monitoring sites in the United States, Atmos. Environ., 62, 646–656, doi:10.1016/j.atmosenv.2012.09.004, 2012.

Lelieveld, J., van Aardenne, J., Fischer, H., de Reus, M., Williams, J. and Winkler, P.: Increasing ozone over the Atlantic Ocean., Science, 304(5676), 1483–7, doi:10.1126/science.1096777, 2004.

Levy, H., Mahlman, J. D., Moxim, W. J. and Liu, S. C.: Tropospheric ozone: The role of transport, J. Geophys. Res., 90(D2), 3753, doi:10.1029/JD090iD02p03753, 1985.

Liang, Q., Jaeglé, L., Jaffe, D. A., Weiss-Penzias, P., Heckman, A. and Snow, J. A.: Long-range transport of

695 Asian pollution to the northeast Pacific: Seasonal variations and transport pathways of carbon
696 monoxide, J. Geophys. Res. Atmos., 109(D23), n/a–n/a, doi:10.1029/2003JD004402, 2004.

697 Lin, M., Fiore, A. M., Cooper, O. R., Horowitz, L. W., Langford, A. O., Levy, H., Johnson, B. J., Naik, V.,
698 Oltmans, S. J. and Senff, C. J.: Springtime high surface ozone events over the western United States:
699 Quantifying the role of stratospheric intrusions, J. Geophys. Res. Atmos., 117(D21), n/a–n/a,
700 doi:10.1029/2012JD018151, 2012a.

701 Lin, M., Fiore, A. M., Horowitz, L. W., Cooper, O. R., Naik, V., Holloway, J., Johnson, B. J., Middlebrook, A.
702 M., Oltmans, S. J., Pollack, I. B., Ryerson, T. B., Warner, J. X., Wiedinmyer, C., Wilson, J. and Wyman, B.:
703 Transport of Asian ozone pollution into surface air over the western United States in spring, J. Geophys.
704 Res. Atmos., 117(4), 1–20, doi:10.1029/2011JD016961, 2012b.

705 Lin, M., Fiore, A. M., Horowitz, L. W., Langford, A. O., Oltmans, S. J., Tarasick, D. and Rieder, H. E.:
706 Climate variability modulates western US ozone air quality in spring via deep stratospheric intrusions.,
707 Nat. Commun., 6, 7105, doi:10.1038/ncomms8105, 2015.

708 Logan, J. A.: Trends in the vertical distribution of ozone: An analysis of ozonesonde data, J. Geophys.
709 Res., 99(D12), 25553, doi:10.1029/94JD02333, 1994.

710 Logan, J. A., Megretskaia, I. A., Miller, A. J., Tiao, G. C., Choi, D., Zhang, L., Stolarski, R. S., Labow, G. J.,
711 Hollandsworth, S. M., Bodeker, G. E., Claude, H., De Muer, D., Kerr, J. B., Tarasick, D. W., Oltmans, S. J.,
712 Johnson, B., Schmidlin, F., Staehelin, J., Viatte, P. and Uchino, O.: Trends in the vertical distribution of
713 ozone: A comparison of two analyses of ozonesonde data, J. Geophys. Res., 104(D21), 26373,
714 doi:10.1029/1999JD900300, 1999.

715 McDermid, I. S.: Differential absorption lidar systems for tropospheric and stratospheric ozone
716 measurements, Opt. Eng., 30(1), 22, doi:10.1117/12.55768, 1991.

717 McDermid, S., Beyerle, G., Haner, D. a and Leblanc, T.: Redesign and improved performance of the
718 tropospheric ozone lidar at the Jet Propulsion Laboratory Table Mountain Facility., Appl. Opt., 41(36),
719 7550–7555, 2002.

720 Mickley, L. J., Jacob, D. J. and Rind, D.: Uncertainty in preindustrial abundance of tropospheric ozone:
721 Implications for radiative forcing calculations, J. Geophys. Res., 106(D4), 3389,
722 doi:10.1029/2000JD900594, 2001.

723 Monks, P.: Gas-phase radical chemistry in the troposphere, Chem. Soc. Rev., 2005.

724 Naja, M. and Akimoto, H.: Contribution of regional pollution and long-range transport to the Asia-Pacific
725 region: Analysis of long-term ozonesonde data over Japan, J. Geophys. Res., 109(D21), D21306,
726 doi:10.1029/2004JD004687, 2004.

727 Naja, M., Lal, S. and Chand, D.: Diurnal and seasonal variabilities in surface ozone at a high altitude site
728 Mt Abu (24.6??N, 72.7??E, 1680 m asl) in India, Atmos. Environ., 37(30), 4205–4215, doi:10.1016/S1352-
729 2310(03)00565-X, 2003.

730 Neu, J. L., Flury, T., Manney, G. L., Santee, M. L., Livesey, N. J. and Worden, J.: Tropospheric ozone
731 variations governed by changes in stratospheric circulation, Nat. Geosci., 7(5), 340–344,
732 doi:10.1038/ngeo2138, 2014.

733 Oltmans, S. J. and Komhyr, W. D.: Surface ozone distributions and variations from 1973–1984:
734 Measurements at the NOAA Geophysical Monitoring for Climatic Change Baseline Observatories, J.
735 Geophys. Res., 91(D4), 5229, doi:10.1029/JD091iD04p05229, 1986.

736 Oltmans, S. J., Lefohn, A. S., Scheel, H. E., Harris, J. M., Levy, H., Galbally, I. E., Brunke, E.-G., Meyer, C. P.,
737 Lathrop, J. A., Johnson, B. J., Shadwick, D. S., Cuevas, E., Schmidlin, F. J., Tarasick, D. W., Claude, H., Kerr,
738 J. B., Uchino, O. and Mohnen, V.: Trends of ozone in the troposphere, Geophys. Res. Lett., 25(2), 139–
739 142, doi:10.1029/97GL03505, 1998.

740 Oltmans, S. J., Lefohn, A. S., Harris, J. M., Galbally, I., Scheel, H. E., Bodeker, G., Brunke, E., Claude, H.,
741 Tarasick, D., Johnson, B. J., Simmonds, P., Shadwick, D., Anlauf, K., Hayden, K., Schmidlin, F., Fujimoto, T.,
742 Akagi, K., Meyer, C., Nichol, S., Davies, J., Redondas, A. and Cuevas, E.: Long-term changes in
743 tropospheric ozone, Atmos. Environ., 40(17), 3156–3173, doi:10.1016/j.atmosenv.2006.01.029, 2006.

744 Oltmans, S. J., Lefohn, a. S., Shadwick, D., Harris, J. M., Scheel, H. E., Galbally, I., Tarasick, D. W.,
745 Johnson, B. J., Brunke, E. G., Claude, H., Zeng, G., Nichol, S., Schmidlin, F., Davies, J., Cuevas, E.,
746 Redondas, a., Naoe, H., Nakano, T. and Kawasato, T.: Recent tropospheric ozone changes - A pattern
747 dominated by slow or no growth, Atmos. Environ., 67, 331–351, doi:10.1016/j.atmosenv.2012.10.057,
748 2013.

749 Parrish, D. D., Millet, D. B., Goldstein, A. H. and Division, C. S.: Increasing ozone in marine boundary layer
750 in ow at the west coasts of North America and Europe, Atmos. Chem. Phys., 1303–1323,
751 doi:10.5194/acp-9-1303-2009, 2009.

752 Parrish, D. D., Law, K. S., Staehelin, J., Derwent, R., Cooper, O. R., Tanimoto, H., Volz-Thomas, A., Gilge,
753 S., Scheel, H.-E., Steinbacher, M. and Chan, E.: Long-term changes in lower tropospheric baseline ozone
754 concentrations at northern mid-latitudes, Atmos. Chem. Phys., 12(23), 11485–11504, doi:10.5194/acp-
755 12-11485-2012, 2012.

756 Petetin, H., Thouret, V., Fontaine, A., Sauvage, B., Athier, G., Blot, R., Boulanger, D., Cousin, J.-M. and
757 Nedelec, P.: Characterizing tropospheric ozone and CO around Frankfurt between 1994–2012 based on
758 MOZAIC-IAGOS aircraft measurements, Atmos. Chem. Phys. Discuss., 15(17), 23841–23891,
759 doi:10.5194/acpd-15-23841-2015, 2015.

760 Pochanart, P., Hirokawa, J. and Kajii, Y.: Influence of regional-scale anthropogenic activity in northeast
761 Asia on seasonal variations of surface ozone and carbon monoxide observed at Oki, Japan, J. Geophys.
762 …, 1999.

763 Reidmiller, D. R., Fiore, A. M., Jaffe, D. A., Bergmann, D., Cuvelier, C., Dentener, F. J., Duncan, B. N.,
764 Folberth, G., Gauss, M., Gong, S., Hess, P., Jonson, J. E., Keating, T., Lupu, A., Marmer, E., Park, R.,
765 Schultz, M. G., Shindell, D. T., Szopa, S., Vivanco, M. G., Wild, O. and Zuber, A.: The influence of foreign
766 vs. North American emissions on surface ozone in the US, Atmos. Chem. Phys., 9(14), 5027–5042,
767 doi:10.5194/acp-9-5027-2009, 2009.

768 Roelofs, G.-J. and Lelieveld, J.: Model study of the influence of cross-tropopause O3 transports on
769 tropospheric O3 levels, Tellus B, 49(1), 38–55, doi:10.1034/j.1600-0889.49.issue1.3.x, 1997.

770 Simmonds, P. G., Derwent, R. G., Manning, A. L. and Spain, G.: Significant growth in surface ozone at
771 Mace Head, Ireland, 1987–2003, Atmos. Environ., 38(28), 4769–4778,
772 doi:10.1016/j.atmosenv.2004.04.036, 2004.

773 Smit, H. G. J., Straeter, W., Johnson, B. J., Oltmans, S. J., Davies, J., Tarasick, D. W., Hoegger, B., Stubi, R.,
774 Schmidlin, F. J., Northam, T., Thompson, A. M., Witte, J. C., Boyd, I. and Posny, F.: Assessment of the
775 performance of ECC-ozonesondes under quasi-flight conditions in the environmental simulation
776 chamber: Insights from the Juelich Ozone Sonde Intercomparison Experiment (JOSIE), J. Geophys. Res.,
777 112(D19), D19306, doi:10.1029/2006JD007308, 2007.

778 Sprenger, M.: A northern hemispheric climatology of cross-tropopause exchange for the ERA15 time
779 period (1979–1993), J. Geophys. Res., 108(D12), 8521, doi:10.1029/2002JD002636, 2003.

780 Staehelin, J., Thudium, J., Buehler, R., Volz-Thomas, A. and Graber, W.: Trends in surface ozone
781 concentrations at Arosa (Switzerland), Atmos. Environ., 28(1), 75–87, doi:10.1016/1352-2310(94)90024-
782 8, 1994.

783 Stevenson, D. S., Dentener, F. J., Schultz, M. G., Ellingsen, K., van Noije, T. P. C., Wild, O., Zeng, G.,
784 Amann, M., Atherton, C. S., Bell, N., Bergmann, D. J., Bey, I., Butler, T., Cofala, J., Collins, W. J., Derwent,
785 R. G., Doherty, R. M., Drevet, J., Eskes, H. J., Fiore, A. M., Gauss, M., Hauglustaine, D. A., Horowitz, L. W.,
786 Isaksen, I. S. A., Krol, M. C., Lamarque, J.-F., Lawrence, M. G., Montanaro, V., Müller, J.-F., Pitari, G.,
787 Prather, M. J., Pyle, J. A., Rast, S., Rodriguez, J. M., Sanderson, M. G., Savage, N. H., Shindell, D. T.,
788 Strahan, S. E., Sudo, K. and Szopa, S.: Multimodel ensemble simulations of present-day and near-future
789 tropospheric ozone, J. Geophys. Res., 111(D8), D08301, doi:10.1029/2005JD006338, 2006.

790 Stohl, A.: On the pathways and timescales of intercontinental air pollution transport, J. Geophys. Res.,
791 107(D23), 4684, doi:10.1029/2001JD001396, 2002.

792 Stohl, A.: Stratosphere-troposphere exchange: A review, and what we have learned from STACCATO, J.
793 Geophys. Res., 108(D12), 8516, doi:10.1029/2002JD002490, 2003.

794 Strode, S. A., Rodriguez, J. M., Logan, J. A., Cooper, O. R., Witte, J. C., Lamsal, L. N., Damon, M., Van
795 Aartsen, B., Steenrod, S. D. and Strahan, S. E.: Trends and variability in surface ozone over the United
796 States, J. Geophys. Res. Atmos., 120(17), n/a–n/a, doi:10.1002/2014JD022784, 2015.

797 Tanimoto, H., Ohara, T. and Uno, I.: Asian anthropogenic emissions and decadal trends in springtime
798 tropospheric ozone over Japan: 1998–2007, Geophys. Res. Lett., 36(23), L23802,
799 doi:10.1029/2009GL041382, 2009.

800 The Royal Society, T.: Ground-level ozone in the 21st century: future trends, impacts and policy
801 implications., 2008.

802 Thompson, A. M., Stone, J. B., Witte, J. C., Miller, S. K., Oltmans, S. J., Kucsera, T. L., Ross, K. L., Pickering,
803 K. E., Merrill, J. T., Forbes, G., Tarasick, D. W., Joseph, E., Schmidlin, F. J., McMillan, W. W., Warner, J.,
804 Hintsa, E. J. and Johnson, J. E.: Intercontinental Chemical Transport Experiment Ozonesonde Network
805 Study (IONS) 2004: 2. Tropospheric ozone budgets and variability over northeastern North America, J.
806 Geophys. Res., 112(D12), D12S13, doi:10.1029/2006JD007670, 2007.

807 Tie, X., Geng, F., Peng, L., Gao, W. and Zhao, C.: Measurement and modeling of O3 variability in
808 Shanghai, China: Application of the WRF-Chem model, Atmos. Environ., 43(28), 4289–4302,
809 doi:10.1016/j.atmosenv.2009.06.008, 2009.

810 Trickl, T., Feldmann, H., Kanter, H.-J., Scheel, H.-E., Sprenger, M., Stohl, A. and Wernli, H.: Forecasted
811 deep stratospheric intrusions over Central Europe: case studies and climatologies, Atmos. Chem. Phys.,
812 10(2), 499–524, doi:10.5194/acp-10-499-2010, 2010.

813 Trickl, T., Bärtsch-Ritter, N., Eisele, H., Furger, M., Mücke, R., Sprenger, M. and Stohl, A.: High-ozone
814 layers in the middle and upper troposphere above Central Europe: potential import from the
815 stratosphere along the subtropical jet stream, Atmos. Chem. Phys., 11(17), 9343–9366, doi:10.5194/acp-
816 11-9343-2011, 2011.

817 Tsutsumi, Y. and Matsueda, H.: Relationship of ozone and CO at the summit of Mt. Fuji (35.35°N,
818 138.73°E, 3776m above sea level) in summer 1997, Atmos. Environ., 34(4), 553–561, doi:10.1016/S1352-
819 2310(99)00238-1, 2000.

820 Vaughan, G., Price, J. D. and Howells, A.: Transport into the troposphere in a tropopause fold, Q. J. R.
821 Meteorol. Soc., 120(518), 1085–1103, doi:10.1002/qj.49712051814, 1994.

822 Volz, A. and Kley, D.: Evaluation of the Montsouris series of ozone measurements made in the
823 nineteenth century, Nature, 332(6161), 240–242, doi:10.1038/332240a0, 1988.

824 Wang, T., Ding, A., Gao, J. and Wu, W. S.: Strong ozone production in urban plumes from Beijing, China,
825 Geophys. Res. Lett., 33(21), L21806, doi:10.1029/2006GL027689, 2006.

826 WMO, M.: A three-dimensional science: Second session of the commission for aerology, WMO Bull., IV,
827 1957.

828 World Health Organization: Health aspects of air pollution with particulate matter, ozone and nitrogen
829 dioxide: report on a WHO working group, Bonn, Germany 13-15 January 2003., 2003.

830 Yates, E. L., Iraci, L. T., Roby, M. C., Pierce, R. B., Johnson, M. S., Reddy, P. J., Tadić, J. M., Loewenstein,
831 M. and Gore, W.: Airborne observations and modeling of springtime stratosphere-to- troposphere
832 transport over California, Atmos. Chem. Phys., 13(24), 12481–12494, doi:10.5194/acp-13-12481-2013,
833 2013.

834 Young, P. J., Archibald, A. T., Bowman, K. W., Lamarque, J.-F., Naik, V., Stevenson, D. S., Tilmes, S.,
835 Voulgarakis, A., Wild, O., Bergmann, D., Cameron-Smith, P., Cionni, I., Collins, W. J., Dalsøren, S. B.,
836 Doherty, R. M., Eyring, V., Faluvegi, G., Horowitz, L. W., Josse, B., Lee, Y. H., MacKenzie, I. A., Nagashima,
837 T., Plummer, D. A., Righi, M., Rumbold, S. T., Skeie, R. B., Shindell, D. T., Strode, S. A., Sudo, K., Szopa, S.
838 and Zeng, G.: Pre-industrial to end 21st century projections of tropospheric ozone from the Atmospheric
839 Chemistry and Climate Model Intercomparison Project (ACCMIP), Atmos. Chem. Phys., 13(4), 2063–
840 2090, doi:10.5194/acp-13-2063-2013, 2013.

841 Zbinden, R. M., Cammas, J.-P., Thouret, V., Nédélec, P., Karcher, F. and Simon, P.: Mid-latitude
842 tropospheric ozone columns from the MOZAIC program: climatology and interannual variability, Atmos.
843 Chem. Phys., 6(4), 1053–1073, doi:10.5194/acp-6-1053-2006, 2006.

844 Zhang, L., Jacob, D. J., Liu, X., Logan, J. A., Chance, K., Eldering, A. and Bojkov, B. R.: Intercomparison
845 methods for satellite measurements of atmospheric composition: application to tropospheric ozone
846 from TES and OMI, Atmos. Chem. Phys., 10(10), 4725–4739, doi:10.5194/acp-10-4725-2010, 2010.

847

848

849

850

Tables:

Table 1. Number of measurements, by month and years, performed at TMF with the tropospheric ozone DIAL system distributed

	Jan	Feb	Mar	Apr	May	Jun	Jul	Aug	Sep	Oct	Nov	Dec	Total
2000	4	2	6	4	11	12	7	10	8	1	4	2	65
2001	1	11	17	2	9	13	12	15	15	17	1	11	130
2002	6	10	6	4	0	10	11	1	6	16	6	10	93
2003	11	9	15	12	10	13	5	7	9	14	11	9	117
2004	9	8	15	14	12	6	12	13	11	10	9	8	130
2005	4	6	13	8	12	16	9	2	7	2	4	6	99
2006	11	9	6	8	14	5	2	12	12	20	11	9	106
2007	0	0	4	9	11	7	8	10	8	26	0	0	101
2008	7	11	8	13	9	4	11	10	6	11	7	11	100
2009	14	11	7	5	7	8	4	10	4	17	14	11	91
2010	0	0	3	8	0	7	4	1	4	5	0	0	44
2011	2	6	4	7	7	11	10	12	7	8	2	6	90
2012	0	9	9	1	10	13	3	2	5	8	0	9	69
2013	6	3	5	10	8	7	5	7	0	0	6	3	51
2014	9	2	5	10	13	16	15	11	15	15	14	6	131
2015	9	15	12	18	3	15	12	NA	NA	NA	NA	NA	83
Total	93	112	135	133	136	162	130	123	117	170	103	86	1500

Table 2. Ozone mixing ratio trends for the median, 5th and 95th percentiles as shown in Figure 6 (see text for details) in ppbv/year (%/year). Statistically significant trends are marked in bold font

< 17-19 km year 5th and 95th , spring and winter out of order? 7-10km winter out of order?>

	Year			Spring			Summer			Fall			Winter		
	Med.	**5th P.**	**95th P.**	**Med.**	**5th P.**	**95th P.**	**Med.**	**5th P.**	**95th P.**	**Med.**	**5th P.**	**95th P.**	**Med.**	**5th P.**	**95th P.**
17-19 km	-0.49 (-0.05)	0.25 (0.05)	-5.37 (-0.37)	-1.01 (-0.1)	3.47 (0.68)	-5.89 (-0.41)	-2.93 (-0.44)	-3.25 (-0.63)	-0.13 (-0.01)	**-8.79** (**-1.39**)	**-5.80** (**-1.26**)	-6.58 (-0.68)	-0.12 (-0.01)	1.37 (0.27)	-21.86 (-1.51)
12-16 km	1.56 (1.01)	-0.01 (-0.01)	2.52 (0.51)	1.10 (0.50)	0.58 (0.19)	0.29 (0.05)	0.08 (0.06)	0.20 (0.30)	0.19 (0.06)	-0.83 (-0.71)	-1.12 (-1.83)	-1.49 (-0.63)	2.54 (1.31)	0.51 (0.65)	0.95 (0.18)
7-10 km	**0.31** (**0.57**)	0.01 (0.03)	**0.55** (**0.54**)	**0.71** (**1.10**)	0.20 (0.49)	4.31 (6.69)	**0.58** (**0.98**)	0.27 (0.90)	1.01 (0.95)	-0.03 (-0.06)	-0.49 (1.62)	0.18 (0.22)	**-0.43** (**-0.87**)	-0.30 (-0.91)	-1.19 (-1.41)
4-7 km	-0.14 (-0.26)	-0.33 (-0.85)	0.19 (0.17)	0.12 (0.20)	-0.29 (-0.67)	0.96 (1.17)	-0.14 (-0.24)	-0.03 (0.09)	-0.01 (-0.01)	-0.23 (0.45)	-0.82 (-2.33)	0.26 (0.06)	**-0.36** (**-0.72**)	**-0.59** (**-1.53**)	0.05 (0.08)

Formatted: Superscript

Formatted: Superscript

Table 3. Number of air parcels ending at TMF during lidar measurements over the period 2000-2015, classified as "Stratosphere", "Central America, "ABL","AFT" and "Pacific Ocean" (see text for details) <Spell out ABL and AFT.>

	Strat	Cent. Am	ABL	AFT	Pac
14 km	1150 (78%)	47 (3%)	0 (0%)	5 (0%)	270 (18%)
13 km	853 (58%)	69 (5%)	1 (0%)	20 (1%)	519 (35%)
12 km	515 (35%)	86 (6%)	4 (0%)	61 (4%)	798 (54%)
11 km	321 (22%)	89 (6%)	16 (1%)	51 (3%)	985 (67%)
10 km	199 (13%)	94 (6%)	17 (1%)	93 (6%)	1058 (71%)
9 km	118 (8%)	98 (7%)	18 (1%)	92 (6%)	1146 (77%)
8 km	70 (5%)	103 (7%)	19 (1%)	82 (6%)	1197 (91%)
7 km	62 (4%)	110 (7%)	19 (1%)	84 (6%)	1194 (81%)
6 km	24 (2%)	133 (9%)	11 (1%)	67 (5%)	1226 (83%)
5 km	31 (2%)	161 (11%)	12 (1%)	87 (6%)	1169 (79%)

Figure captions:

Figure 1. a) Profile of the mean relative difference between the lidar and the ECC ozone number density for the 32 simultaneous measurements (dark blue). Lidar uncertainty (light blue) and mean relative difference obtained between 4 and 16 km (red dotted line) are superimposed. The black solid curve shows the number of data points at each altitude. b) Histogram of the difference between the lidar and the ECC ozone number density. c) Column-averaged (below 8 km) difference between the lidar and the ECC sonde for each coincidence

Figure 2. a) Composite monthly mean surface ozone at TMF and nearby ARB stations obtained from hourly samples (left) and 8hMDA values (right) for the period 2013-2015. b) Composite mean ozone daily cycle at TMF and nearby ARB stations for the four seasons for the period 2013-2015

Figure 3. a) Ozone mixing ratio climatological average (2000-2015) computed from the TMF lidar measurements (red curve). The cyan horizontal bars indicate the standard deviation at intervals of 1-km. The red dot at the bottom indicates the mean surface ozone mixing ratio (2013-2015) measured simultaneously with lidar. b) Seasonally-averaged ozone mixing ratio profiles for spring (MAM), summer (JJA), fall (SON) and winter (DJF). The dots at the bottom indicate the corresponding surface ozone seasonal averages

Figure 4. Composite monthly mean ozone mixing ratio (2000-2015) computed from the TMF lidar measurements. The dashed line indicates the climatological tropopause above the site (WMO definition). Bottom strip: Composite monthly mean ozone mixing ratio (2000-2015) from the surface measurements

Figure 5. Deseasonalized ozone mixing ratio above TMF. Anomalies (in %) were computed with respect to the climatological (2000-2015) monthly mean

Figure 6. Time series of the median (blue), 5th (orange) and 95th (yellow) percentile ozone values at different altitude layers for the full year (top) and for selected seasons and altitude layers (bottom) obtained from the TMF lidar measurements. Dashed lines represent the linear fit for each time series

Figure 7. Geographical boundaries used to characterize the air parcels associated with the 8-day backward trajectories ending at TMF during the lidar measurements over the period 2000-2015

Figure 8. Examples of HYSPLIT 8-day backward trajectories arriving at TMF at 7 km altitude for four selected seasons and categories (see text for details)

Figure 9. Distribution of the five categories identified for each trajectory ending at TMF during the lidar measurements over the period 2000-2015. The number of occurrences is given for each month of the year, and for four different altitude layers

Figure 10. Box plot of the ozone mixing ratios measured within the air masses arriving at TMF at 9 km for the five identified categories (see text for details) and the four seasons. The black dot represents the mean value, the red line is the median and the box limits correspond to the 25th and 75th percentiles. The numbers between parentheses indicate the number of associated trajectories. <ST mean values in Sp. Summer and Winter look high. Summer AFT mean looks high.>

Figure 11. Composite profiles of the ozone mixing ratio associated with the different categories and for each season. Results are shown only when the number of samples for a given category was larger than 5% of the total number of samples in that season

Figure 12. Monthly distribution of occurrences (in %) of double tropopauses above TMF. The number of days with tropopause folds is normalized to the total number of measurements per month compiled in Table1

Figure 13. a) to d) Altitude distribution of the tropopause above TMF for spring, summer, fall and winter respectively, and in the absence of double-tropopause. e) to h) Altitude distribution of the lower (first) tropopause above TMF for spring, summer, fall and winter respectively, and in the presence of a double-tropopause. i) to l) Same as e) to h) but for the upper or second tropopause. All computations were made at the times of the TMF lidar measurements

Figure 14. Winter- (cyan) and Spring- (red) averaged ozone mixing ratio profiles computed in the presence of a double tropopause (DT, solid curves) and single tropopause (ST, dashed curves). The horizontal solid grey curves depicts the average altitude of the lower and upper tropopauses when a double tropopause was identified. The horizontal dashed grey line corresponds to the average altitude of the tropopause when a single tropopause was identified. b) Same as a) but zoomed on the tropospheric part of the profiles (4-10 km)

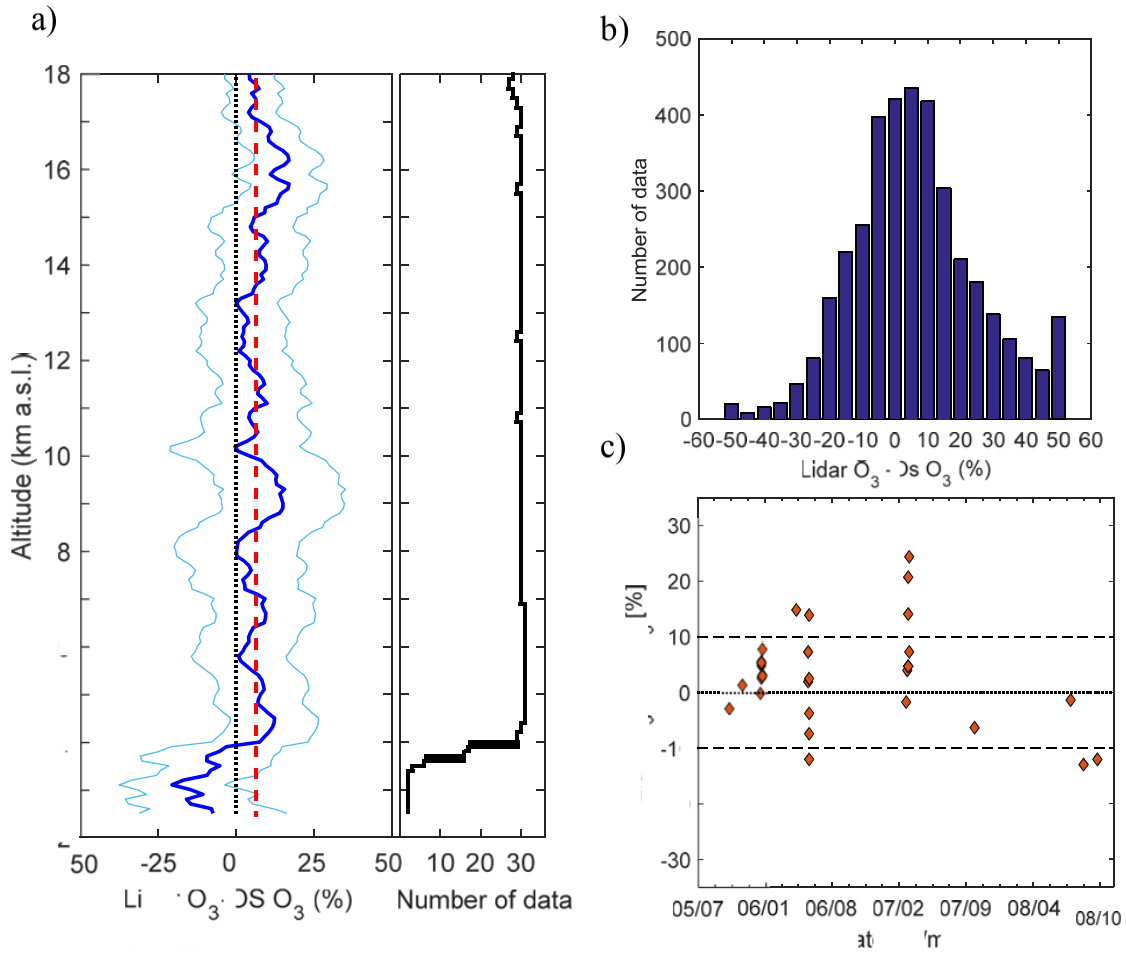
a)
b)
c)
Altitude (km a.s.l.)
Number of data
Number of data
[%]
05/07
06/01
06/08
07/02
07/09
08/04
08/10

a)

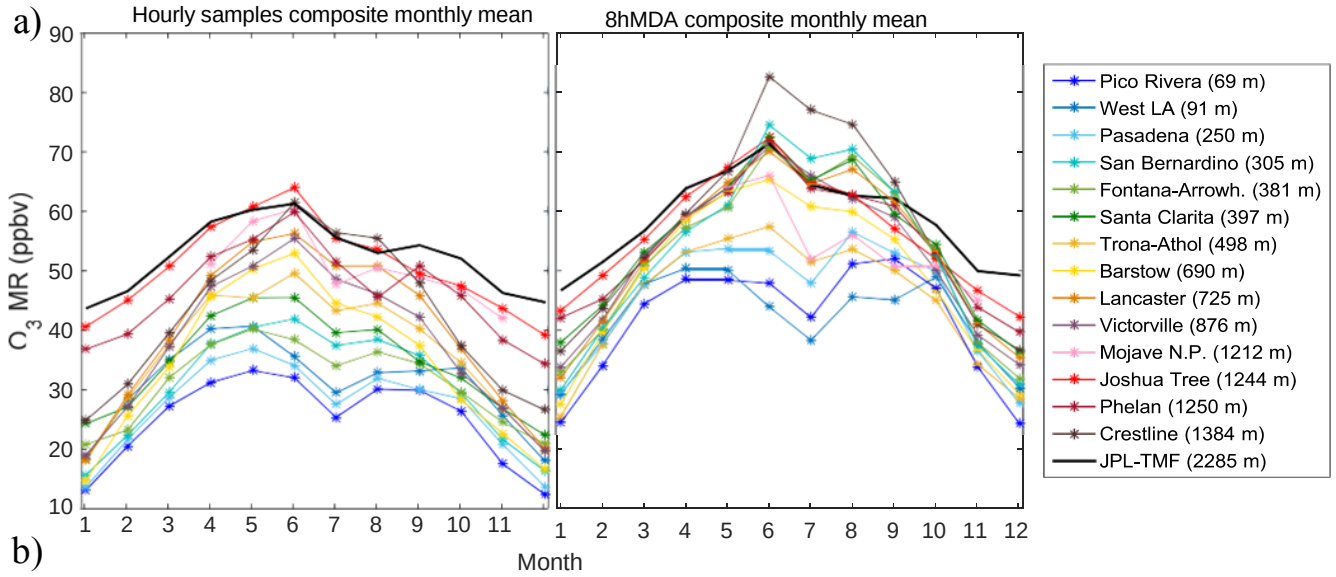
Hourly samples composite monthly mean
8hMDA composite monthly mean
O_3 MR (ppbv)
Month
Pico Rivera (69 m)
West LA (91 m)
Pasadena (250 m)
San Bernardino (305 m)
Fontana-Arrowh. (381 m)
Santa Clarita (397 m)
Trona-Athol (498 m)
Barstow (690 m)
Lancaster (725 m)
Victorville (876 m)
Mojave N.P. (1212 m)
Joshua Tree (1244 m)
Phelan (1250 m)
Crestline (1384 m)
JPL-TMF (2285 m)

b)

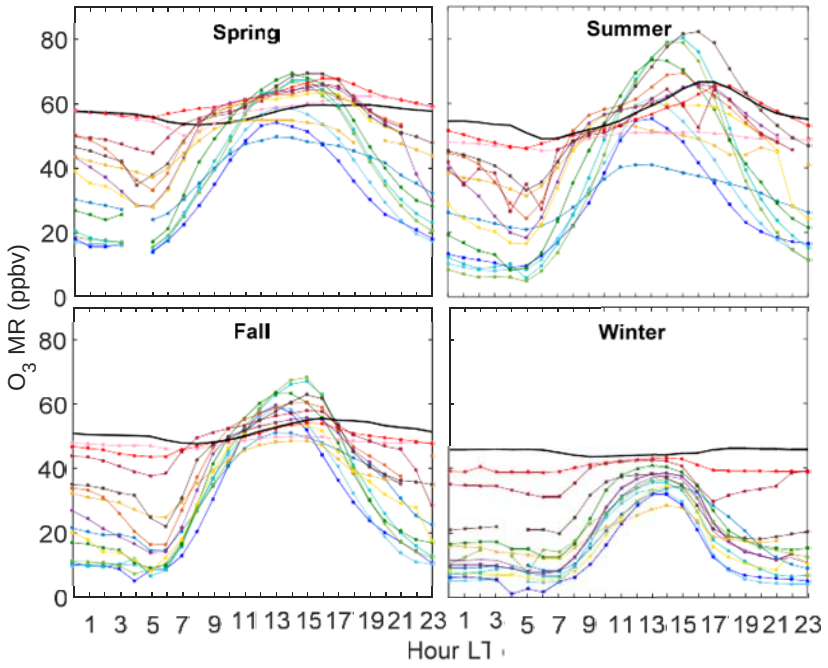
Spring
Summer
Fall
Winter
O_3 MR (ppbv)
Hour LT

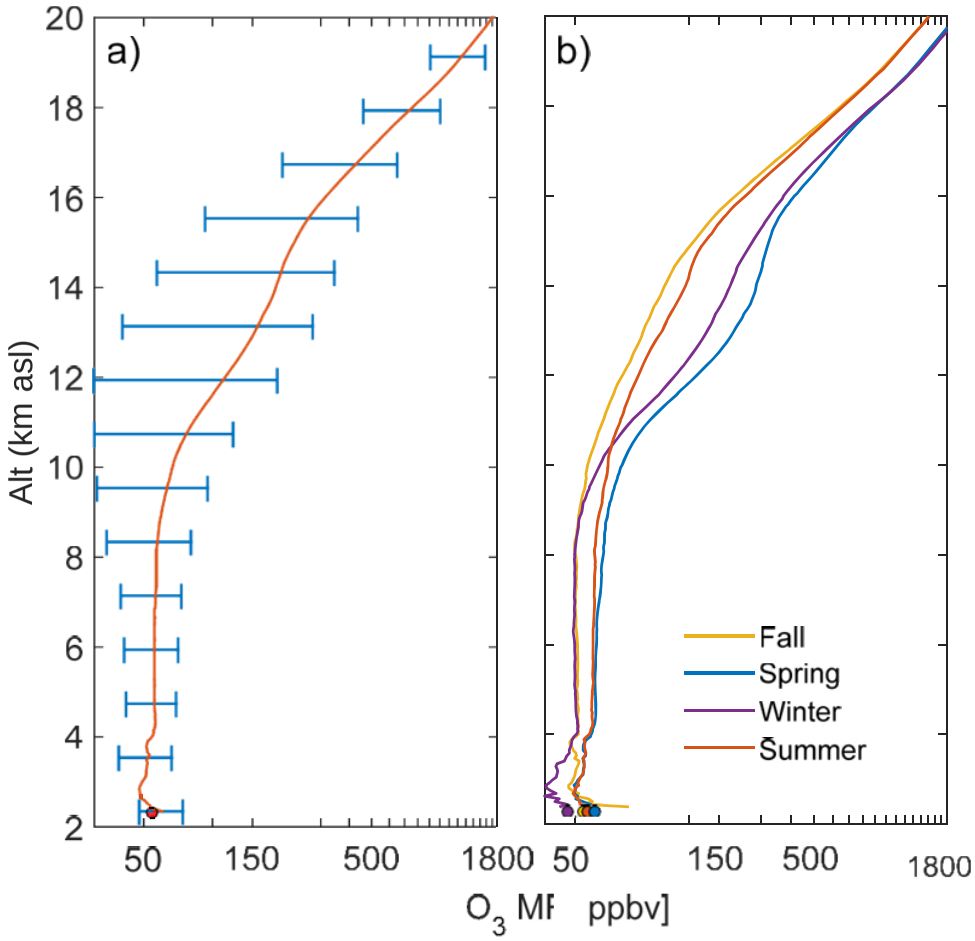
a)
b)
Alt (km asl)
20
18
16
14
12
10
8
6
4
2
50
150
500
1800
50
150
500
1800
Fall
Spring
Winter
Summer
ppbv]

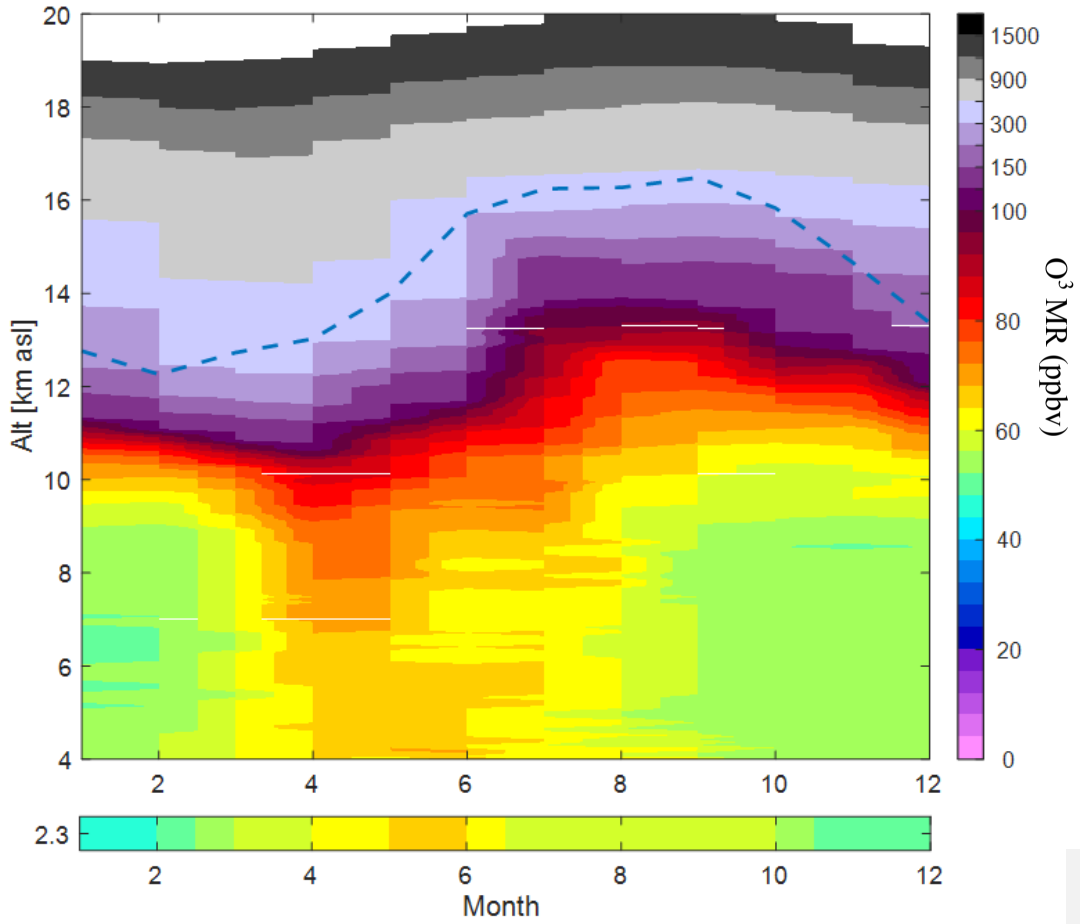
Alt [km asl]
20
18
16
14
12
10
8
6
4
2
4
6
8
10
12
2.3
2
4
6
8
10
12
Month
1500
900
300
150
100
80
60
40
20
0
O3 MR (ppbv)

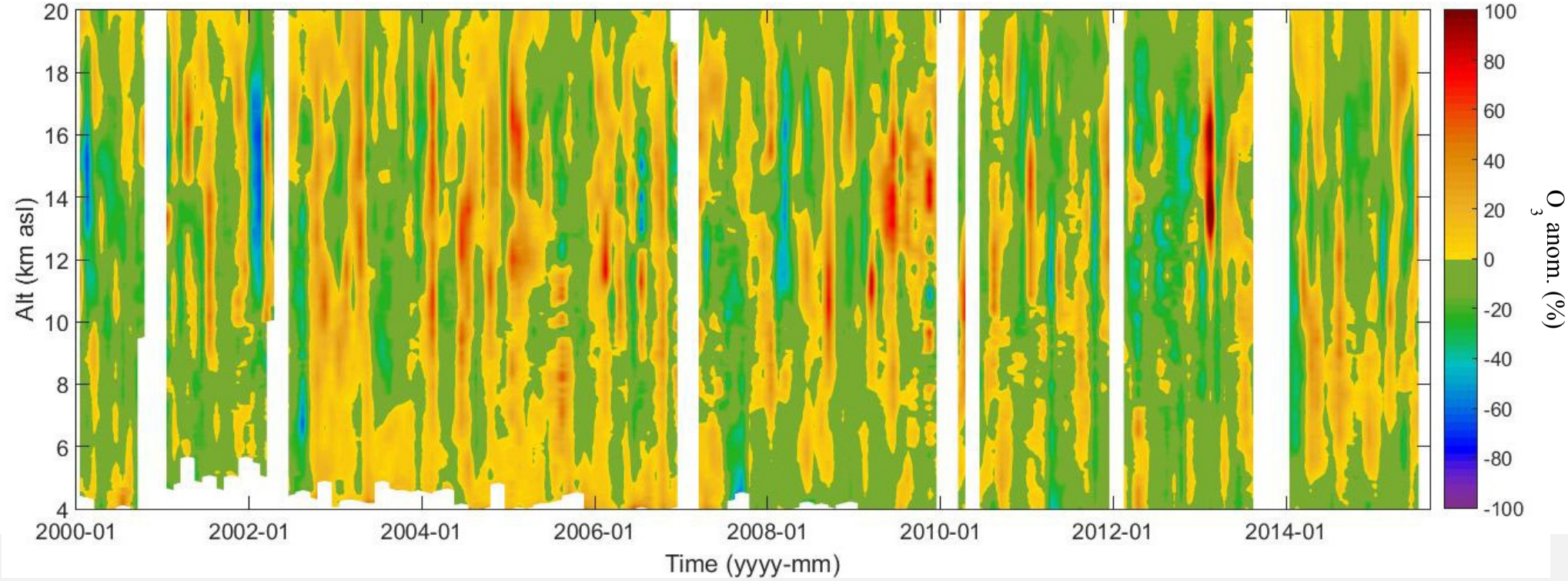
Alt (km asl)
20
18
16
14
12
10
8
6
4
2000-01
2002-01
2004-01
2006-01
2008-01
2010-01
2012-01
2014-01
Time (yyyy-mm)
100
80
60
40
20
0
-20
-40
-60
-80
-100
O3 anom. (%)

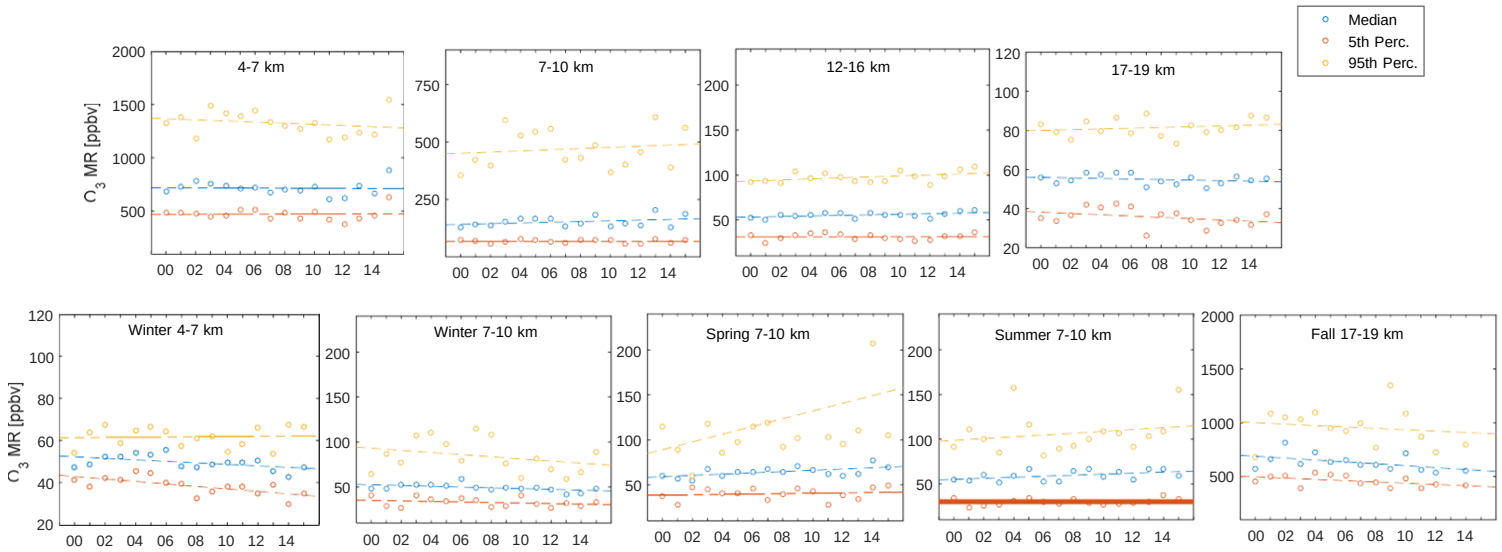
Median
5th Perc.
95th Perc.
4-7 km
7-10 km
12-16 km
17-19 km
Winter 4-7 km
Winter 7-10 km
Spring 7-10 km
Summer 7-10 km
Fall 17-19 km
O_3 MR [ppbv]
00 02 04 06 08 10 12 14

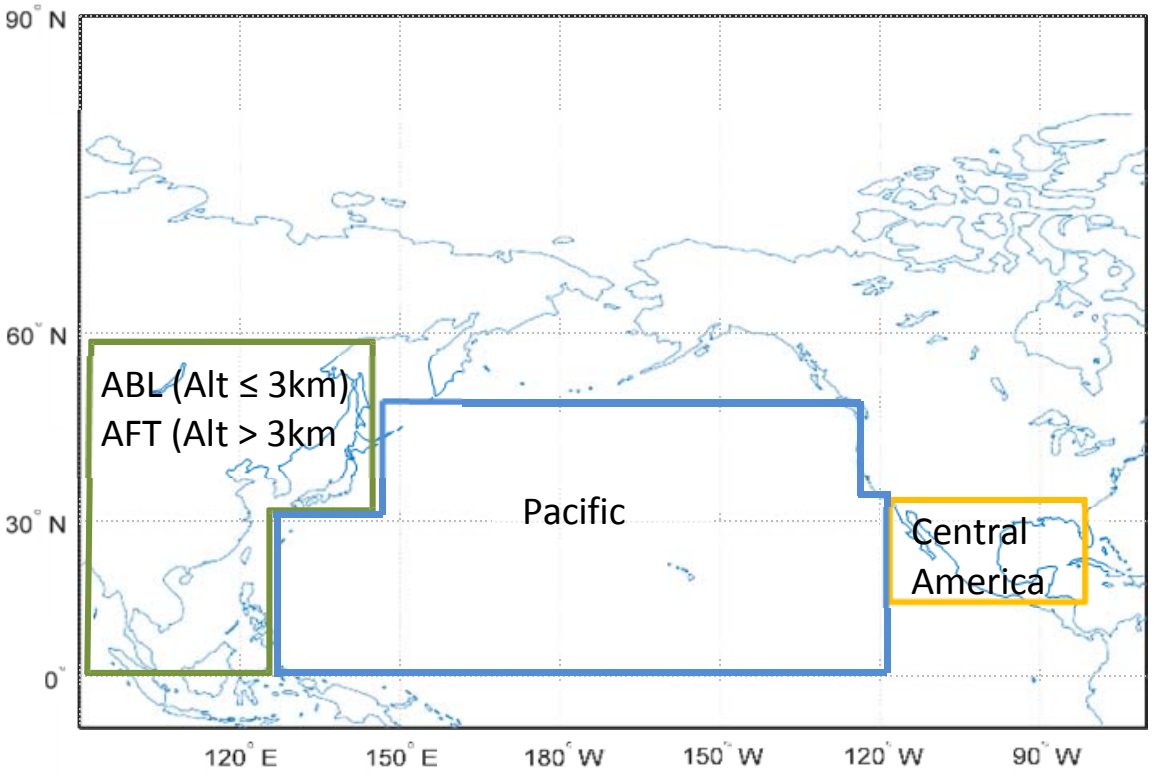
90° N
60° N
30° N
0°
120° E
150° E
180° W
150° W
120° W
90° W
ABL (Alt ≤ 3km)
AFT (Alt > 3km
Pacific
Central America

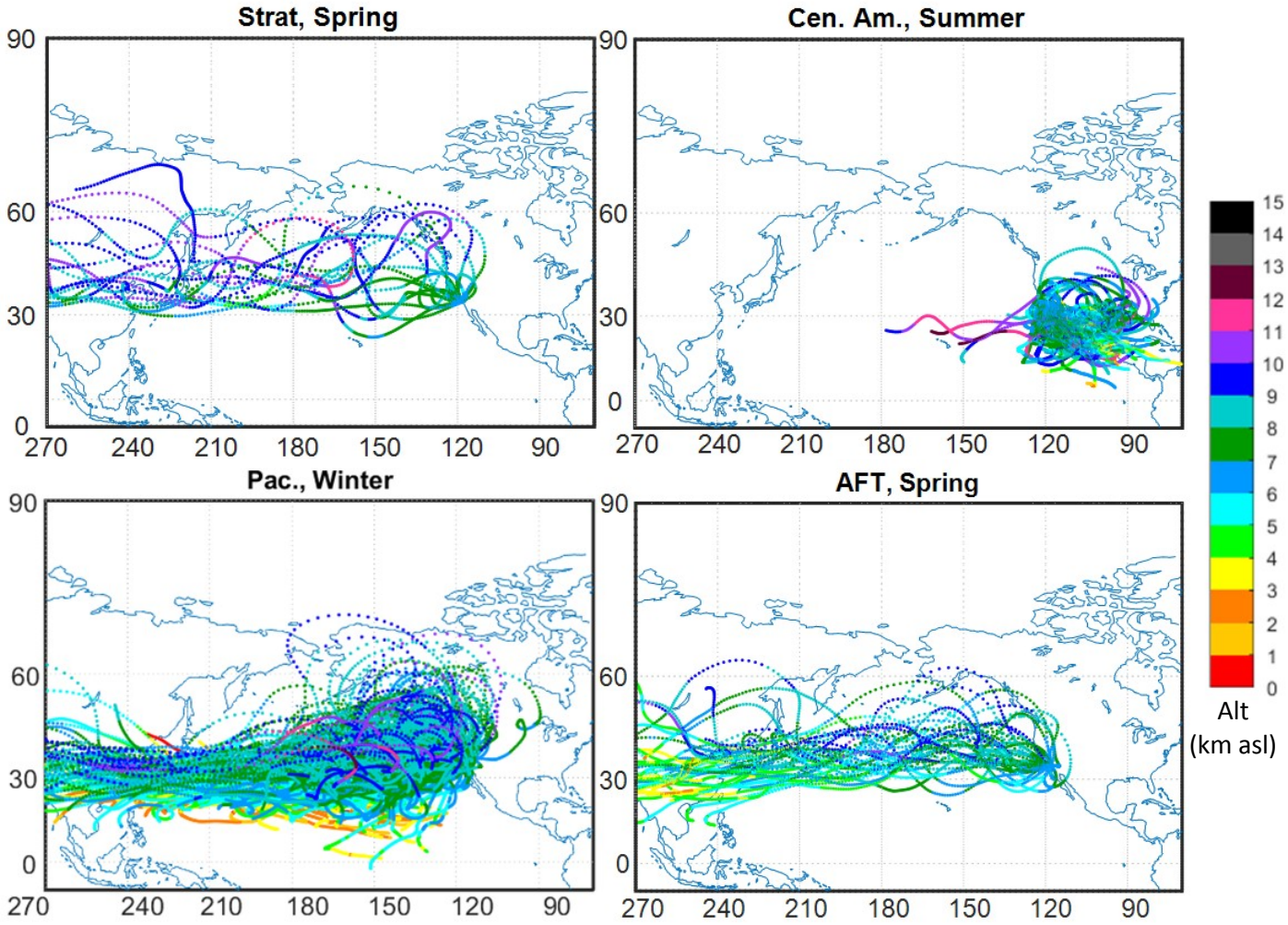
Strat, Spring
Cen. Am., Summer
Pac., Winter
AFT, Spring
90
60
30
0
270
240
210
180
150
120
90
15
14
13
12
11
10
9
8
7
6
5
4
3
2
1
0
Alt
(km asl)

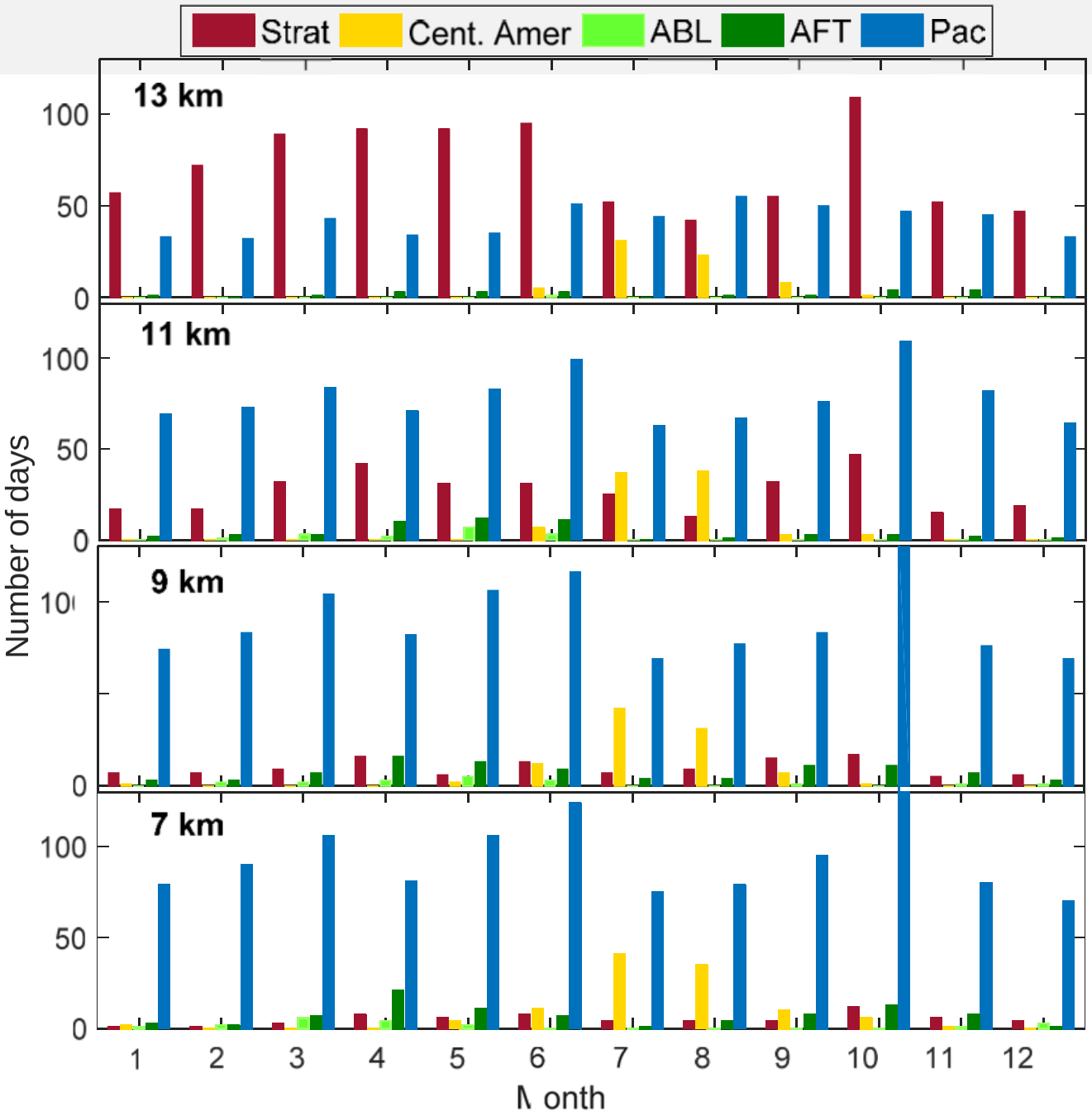
Strat
Cent. Amer
ABL
AFT
Pac
13 km
11 km
9 km
7 km
100
50
0
Number of days
1
2
3
4
5
6
7
8
9
10
11
12
N onth

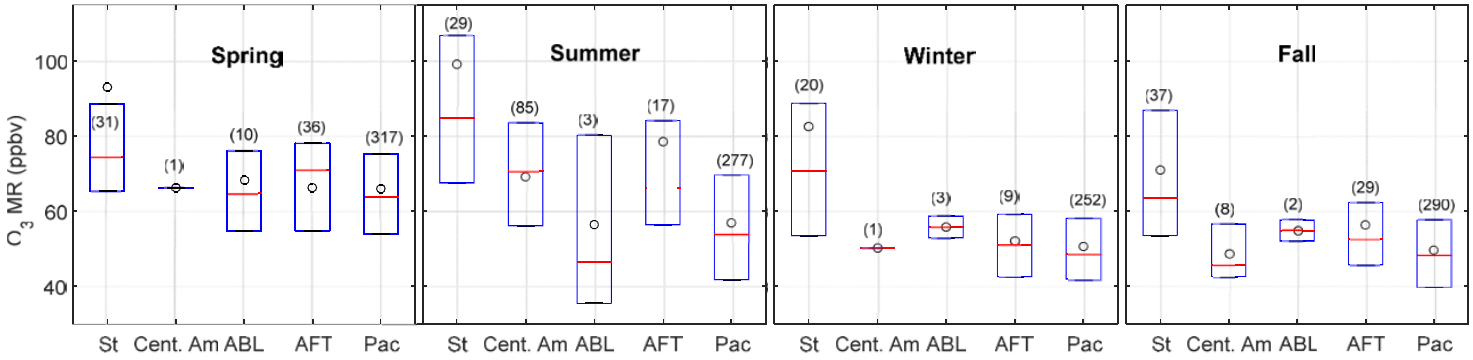
Spring
Summer
Winter
Fall
O_3 MR (ppbv)
100
80
60
40
St
Cent. Am
ABL
AFT
Pac
(31)
(1)
(10)
(36)
(317)
(29)
(85)
(3)
(17)
(277)
(20)
(1)
(3)
(9)
(252)
(37)
(8)
(2)
(29)
(290)

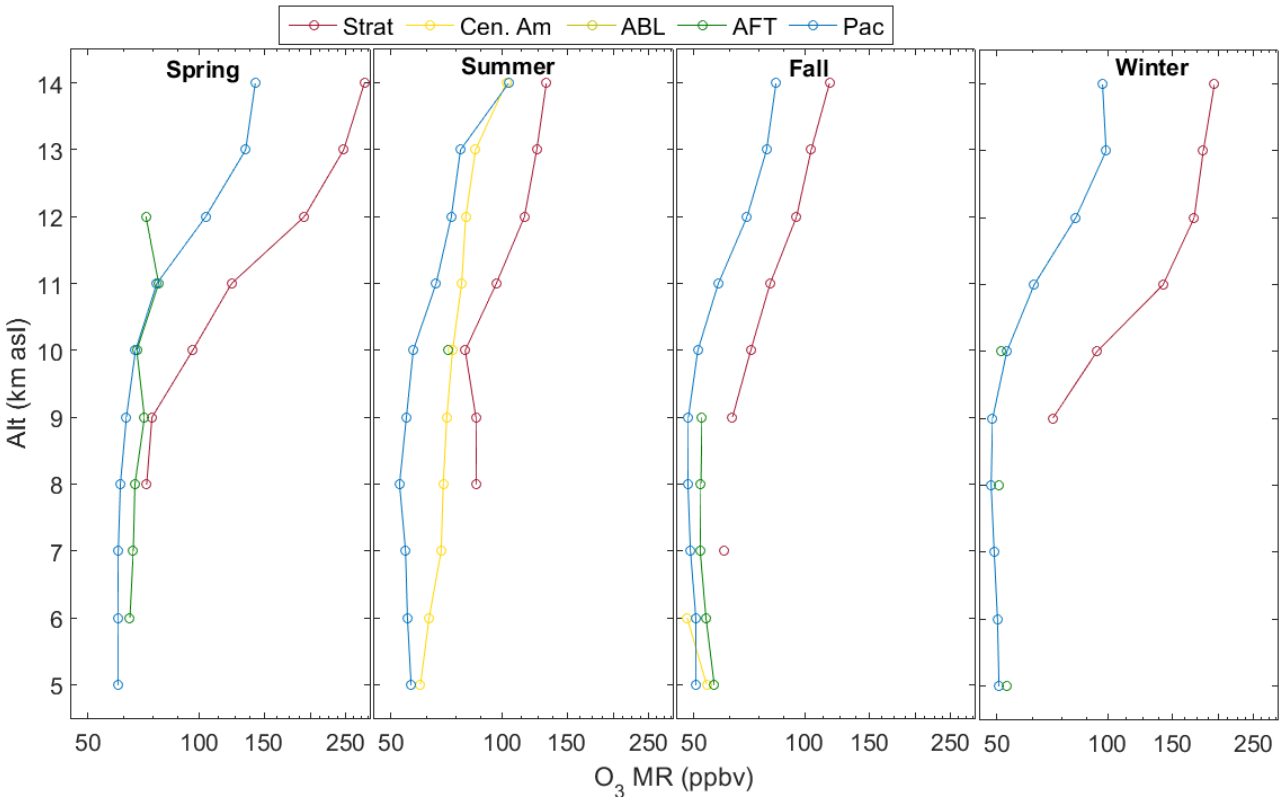
Strat
Cen. Am
ABL
AFT
Pac
Spring
Summer
Fall
Winter
Alt (km asl)
14
13
12
11
10
9
8
7
6
5
50
100
150
250
O3 MR (ppbv)

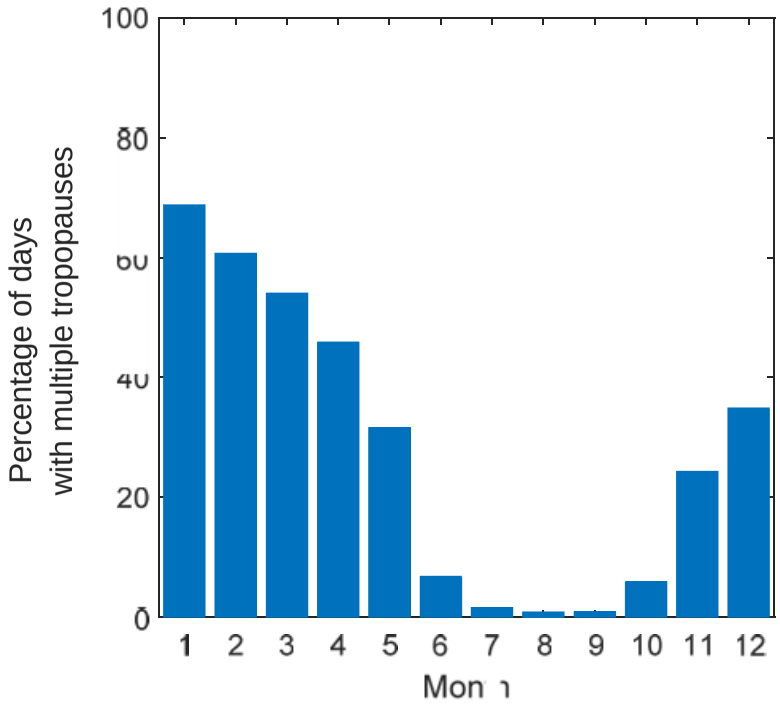
Percentage of days
with multiple tropopauses
100
80
60
40
20
0
1
2
3
4
5
6
7
8
9
10
11
12
Mon

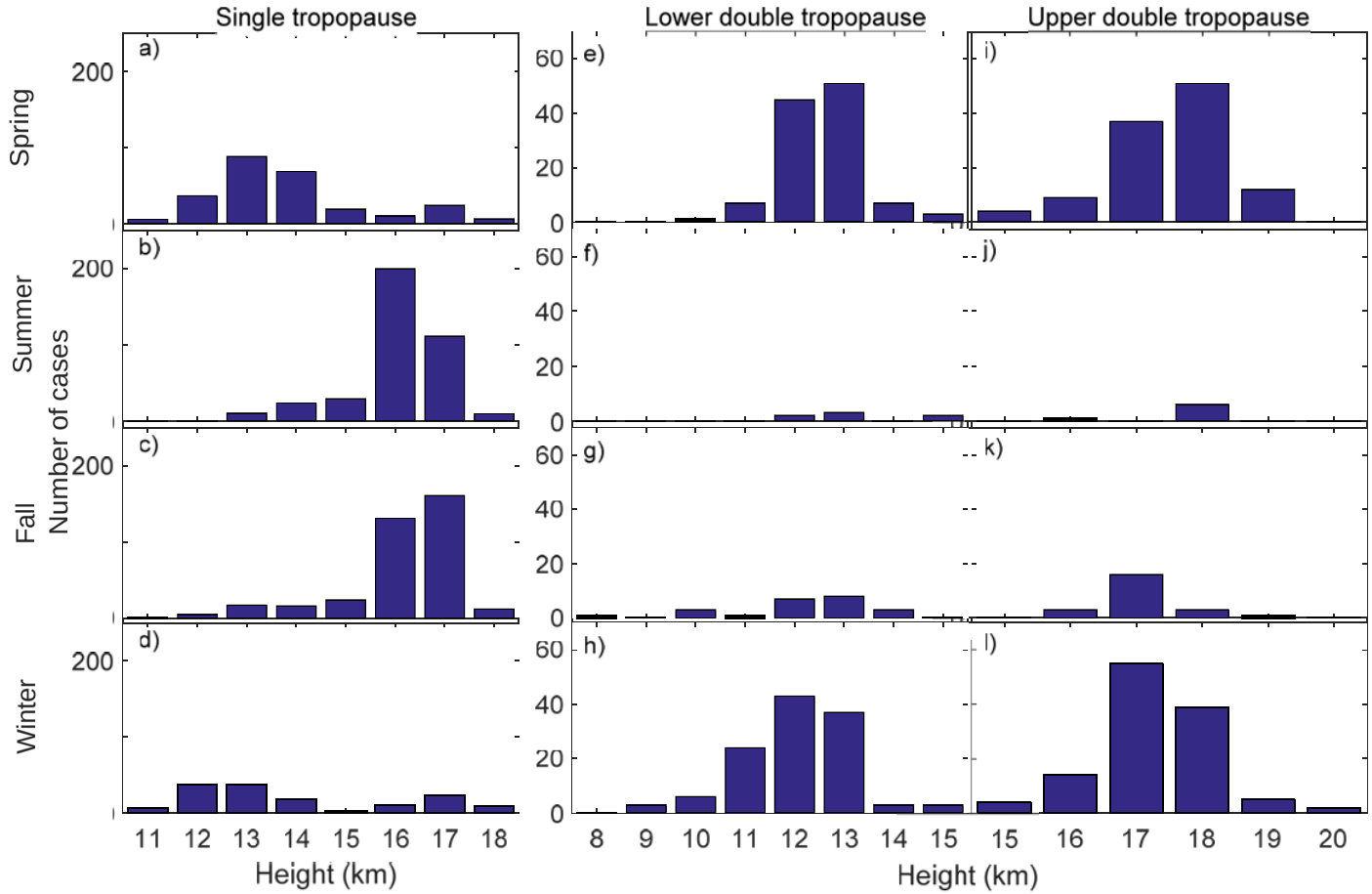
Single tropopause
Lower double tropopause
Upper double tropopause
Spring
Summer
Fall
Winter
Number of cases
a)
b)
c)
d)
e)
f)
g)
h)
i)
j)
k)
l)
200
60
40
20
0
11 12 13 14 15 16 17 18
8 9 10 11 12 13 14 15
15 16 17 18 19 20
Height (km)
Height (km)

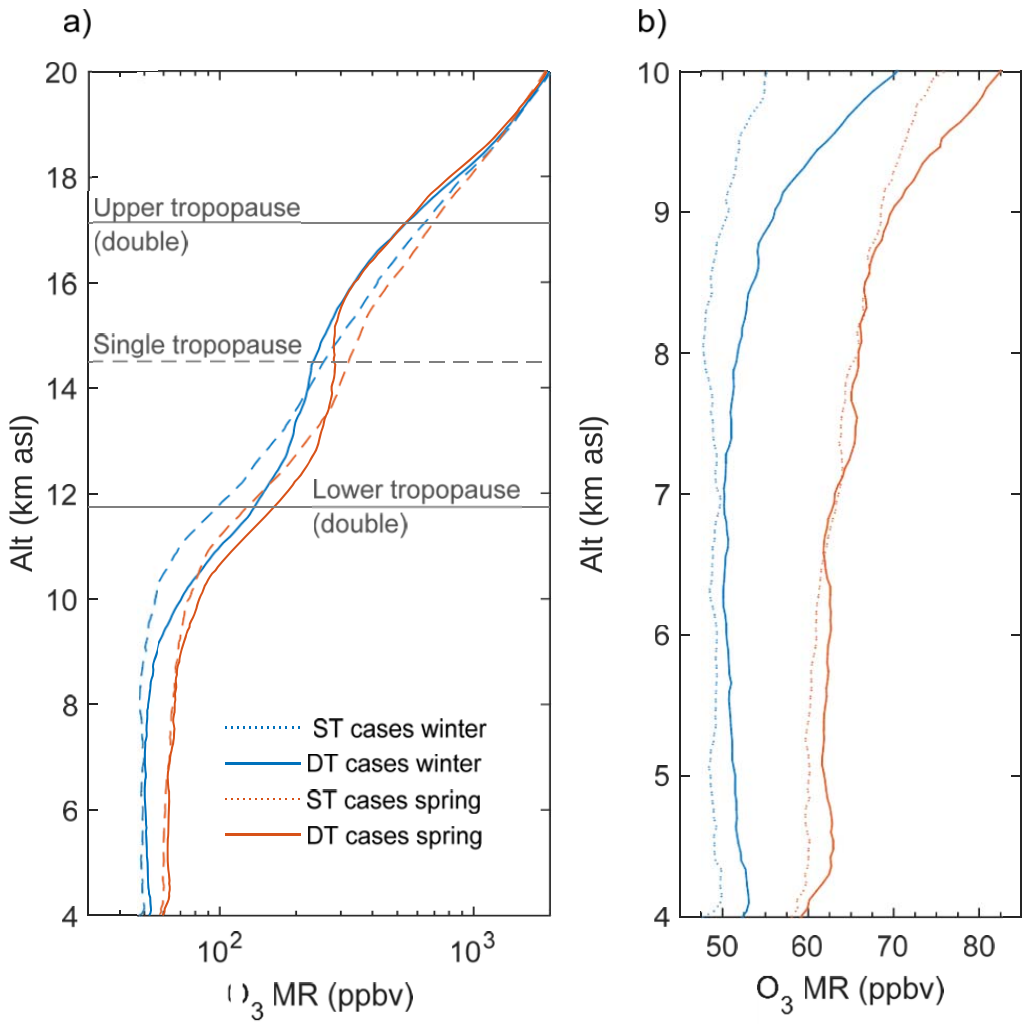
a)
b)
Alt (km asl)
Upper tropopause
(double)
Single tropopause
Lower tropopause
(double)
ST cases winter
DT cases winter
ST cases spring
DT cases spring
10^2
10^3
O_3 MR (ppbv)
50
60
70
80

Newchurch, M. J., M. A. Ayoub, S. Oltmans, B. Johnson, and F. J. Schmidlin (2003), Vertical distribution of ozone at four sites in the United States, *J. Geophys. Res.*, *108*(D1), 4031.
Proffitt, M. H., and A. O. Langford (1997), Ground-based differential absorption lidar system for day or night measurements of ozone throughout the free troposphere, *Appl. Opt.*, *36*(12), 2568-2585.